Lasing thresholds and photon statistics in high-β buried multiple quantum well photonic crystal nanocavity lasers

N. Takemura,[1,2,*] M. Takiguchi,[1,2] E. Kuramochi,[1,2] A. Shinya,[1,2] T. Sato,[3] K. Takeda,[1,3] S. Matsuo,[1,3] and M. Notomi[1,2]

[1]*NTT Nanophotonics Center, NTT Corp., 3-1, Morinosato Wakamiya Atsugi, Kanagawa 243-0198, Japan*

[2]*NTT Basic Research Laboratories, NTT Corp., 3-1, Morinosato Wakamiya Atsugi, Kanagawa 243-0198, Japan*

[3]*NTT Device Technology Laboratories, NTT Corp., 3-1, Morinosato Wakamiya Atsugi, Kanagawa 243-0198, Japan*

(Received 19 October 2018; revised manuscript received 25 January 2019; published 15 May 2019)

We investigate the lasing thresholds and photon statistics of buried multiple quantum well (MQW) photonic crystal (PhC) lasers with a high spontaneous emission coupling coefficient β and a large carrier transparency number N_0. Using measured input-output curves and delay-dependent second-order photon correlations $g^{(2)}(\tau)$, we estimate that our population inversion threshold is near the kink threshold of the input-output curve, which indicates that the buried MQW PhC lasers operate close to the "lasers without inversion" (intensity jump without inversion) regime proposed by Yamamoto and Björk. With respect to static photon statistics $g^{(2)}(0)$, the super-Poissonian photon statistics $g^{(2)}(0) > 1$ are observed even one order of magnitude above the kink threshold. The super-Poissonian photon statistics are specific to the class-B lasers where the photon decay rate γ_c is much larger than that of carriers $\gamma_\parallel$ and the relaxation oscillation occurs. We also propose that the pump power needed to maximize the damping time of the relaxation oscillation could be the noise threshold at which the photon statistics change from thermal to Poissonian.

DOI: 10.1103/PhysRevA.99.053820

I. INTRODUCTION

Advances in nanotechnology have moved cavity quantum electrodynamics (cavity-QED) into the world of semiconductor nanostructures. By combining high-Q photonic crystal (PhC) microcavities with semiconductor active gain materials, photons confined in a cavity interact efficiently with matter. One of the achievements in the weak-coupling cavity-QED regime is thresholdless lasers, where conventional lasing thresholds disappear due to a spontaneous emission coupling factor β of near unity [1,2]. Recently, we succeeded in combining a multiquantum well (MQW) and a high-Q photonic crystal (PhC) nanocavity and realized the Purcell enhancement of the carrier decay rate [3], lasing with current injection [4], and even thresholdless lasing at cryogenic temperatures [5].

Although there have been many experimental and theoretical studies on the lasing properties and photon statistics of high-β lasers [6–21], most experiments have been using lasers with quantum dots (QDs). The lasing thresholds and photon statistics of high-β nanocavity lasers with MQW have not yet been discussed in detail. Of particular interest is the large active mode volume of the MQW structure, which gives rise to a non-negligible carrier transparency number $N_0(\gtrsim 10^4)$. Therefore, our system is very different from QDs where a only small number of emitters (typically 10∼500 emitters) are involved in lasing. In fact, our buried MQW PhC structure is one of few systems that can realize a high β and a large N_0 simultaneously [4,15,22], and N_0 is estimated to be about 10000 in our system. The physics of lasers in high-β and large-N_0 regimes is an interesting field but very little is known because of the difficulty involved in experimental work. For example, the definition of lasing threshold needs to be reconsidered in this region [23]: the widely used gain-loss balance threshold is unsatisfactory. Moreover, in this context, one interesting phenomenon is "lasers without inversion" (intensity jump without inversion), which was proposed by Yamamoto and Björk [24]. When β is close to unity while N_0 remains large, the pump-input and light-output curve exhibits a thresholdlike kink with a pump power that is insufficient to reach population inversion. Furthermore, the photon-statistical properties of lasers in the high-β and large-N_0 regime have not yet been studied intensively. In this paper, we study the lasing thresholds and photon statistics of buried MQW PhC nanocavity lasers and analyze the measured results with simple theoretical models.

First, we estimate physical parameters such as β and N_0 based on measured input-output curves and delay-dependent second-order photon correlation functions $g^{(2)}(\tau)$. In particular, we make use of the damped oscillatory behavior of $g^{(2)}(\tau)$ that originates from the commonly observed relaxation oscillation in semiconductor lasers [25,26]. The oscillation frequency and the damping time of $g^{(2)}(\tau)$ are very sensitive to β and N_0 and provide information on the dynamical properties of lasers. The estimated parameters indicate that, in the measured buried MQW PhC laser, the pump power needed to create a population inversion is comparable to the kink threshold of the input-output curve. This is in striking contrast to conventional low-β lasers where the population inversion is created far below the kink threshold of the input-output curves. Thus, we argue that our laser is very close to the intensity jump without inversion regime due to its high β and large N_0.

Second, we discuss in detail the photon statistics $g^{(2)}(0)$ of the buried MQW PhC lasers. We observe the super-Poissonian

*naotomo.takemura.ws@hco.ntt.co.jp

photon statistics [$g^{(2)}(0) > 1$] that remain even far above the kink threshold of the input-output curve. These are characteristic photon statistics when the photon decay rate γ_c is much larger than the carrier rate $\gamma_\parallel$: $\gamma_c/\gamma_\parallel \gg 1$, which is the photon statistics in the class-B limit studied in Refs. [8,27–31]. The super-Poissonian photon statistics even high above the kink threshold may result from the relaxation oscillation with a long damping time.

Finally, we propose a photon statistics noise threshold with respect to the damping time of the relaxation oscillation. In class-B lasers, no previously proposed definition of the lasing threshold has been able to predict the noise threshold pump power where $g^{(2)}(0)$ changes from thermal to Poissonian statistics. We find that the threshold of $g^{(2)}(0)$ at which $g^{(2)}(0)$ changes from thermal to Poissonian statistics might be characterized as the pump power at which the damping time of the relaxation oscillation reaches maximum.

The outline of this paper is as follows. The theoretical model is introduced in Sec. II. The various definitions of lasing threshold are discussed in Sec. III. We present and analyze our experimental results in Sec. IV. Section V discusses the noise threshold. Finally, Sec. VI provides our conclusions.

II. THEORY

A. Rate equations

To analyze the measurements presented in the next section, we use conventional rate equations, which are a very simple and standard model but have many nontrivial consequences [2,7,8,10,12,20,32]. The rate equations for semiconductor lasers with a linear gain are given by

$$\dot{n} = -\gamma_c n + \beta\gamma_\parallel N + \beta\gamma_\parallel N n - \beta\gamma_\parallel N_0 n \tag{1}$$

$$\dot{N} = -\gamma_\parallel N - \beta\gamma_\parallel N n + \beta\gamma_\parallel N_0 n + P. \tag{2}$$

where n and N are photon and carrier numbers, respectively. The terms $\beta\gamma_\parallel N$, $\beta\gamma_\parallel Nn$, and $\beta\gamma_\parallel N_0 n$, respectively, represent the spontaneous, stimulated, and absorption with a finite carrier transparency number. The photon decay rate is given by γ_c. Meanwhile, the carrier decay rate $\gamma_\parallel$ and the spontaneous coupling coefficient β are, respectively, defined as [7]

$$\gamma_\parallel \equiv \gamma_N + \frac{4g^2}{\gamma_\perp + \delta^2/\gamma_\perp} \tag{3}$$

and

$$\beta \equiv \frac{4g^2}{\gamma_\parallel(\gamma_\perp + \delta^2/\gamma_\perp)} = \frac{\frac{4g^2}{\gamma_\perp+\delta^2/\gamma_\perp}}{\gamma_N + \frac{4g^2}{\gamma_\perp+\delta^2/\gamma_\perp}}. \tag{4}$$

Here, γ_N is the decay rate of carriers without a photon emission to the cavity mode and $\gamma_\perp$ is the dephasing rate. The constant g represents the coupling strength between the polarization of the gain medium and the cavity photons and δ is the energy detuning between the cavity and the gain medium. When deriving the rate equations, the polarization degree of freedom is adiabatically eliminated by assuming that the dephasing rate is much larger than the other decay rates: $\gamma_\perp \gg \gamma_c, \gamma_N$. Since γ_N includes all carrier decay processes that do not emit photons to the cavity mode, in our definition, γ_N includes both the radiative and nonradiative decay rates. When the decay rates satisfy $\gamma_c \gtrsim \gamma_\parallel$, lasers are called class-B lasers [33–35], which is the case for most semiconductor lasers. Meanwhile, when the photon lifetime is larger than the carrier lifetime, lasers will be categorized as class-A lasers. We note that, in some articles, γ_N does not include the nonradiative decay rate and it appears explicitly in the rate equations, thus the definition of β in these articles is different from ours. From Eq. (4), the spontaneous coupling factor β is viewed as a fraction of the carrier decay into the lasing mode (cavity mode). When $\beta = 1$, all spontaneously emitted photons are coupled to the cavity. In fact, $\beta = 1$ is achieved when $\gamma_N = 0$, where carriers decay only through cavity decay via the light-matter interaction.

We also note that, as represented in Eq. (3), $\gamma_\parallel$ is the enhanced carrier decay rate caused by the coupling between the gain medium and the cavity photons g. Actually, the enhancement factor $4g^2/(\gamma_\perp + \delta^2/\gamma_\perp)$ is the large dephasing limit ($\gamma_\perp \gg \gamma_c$) of the generalized Purcell enhancement factor [36]. It is known that when the large dephasing $\gamma_\perp$ is dominant, the Purcell enhancement does not depend on the cavity decay rate (Q factor) [37]. This Purcell enhancement of $\gamma_\parallel$ will be important at cryogenic temperatures, while, at room temperatures, this effect is modest or negligible. In fact, at cryogenic temperatures, we observed the Purcell enhancement with the same structure as in this paper [3], while at room temperatures we could not.

B. Steady state

Let us consider the steady-state properties of the rate equations. Putting $\dot{n} = 0$ and $\dot{N} = 0$ in Eq. (1) and (2), respectively, the steady-state solutions of the photon $\bar{n}$ and carrier number $\bar{N}$ are given by

$$\bar{n} = \frac{1}{2\beta}[-(\xi(1-\beta) + 1 - \beta P/\gamma_c) + \sqrt{(\xi(1-\beta) + 1 - \beta P/\gamma_c)^2 + 4\beta^2 P/\gamma_c}\,] \tag{5}$$

and

$$\bar{N} = \left(\frac{\gamma_c}{\gamma_\parallel}\right)\frac{\xi\bar{n} + P/\gamma_c}{1+\beta\bar{n}} = N_0 + \left(\frac{\gamma_c}{\gamma_\parallel}\right)\frac{P/\gamma_c - \xi/\beta}{1+\beta\bar{n}}. \tag{6}$$

Here, the dimensionless parameter ξ is associated both with the carrier transparency number N_0 and the spontaneous emission coupling factor β as [2]

$$\xi = \beta N_0\left(\frac{\gamma_\parallel}{\gamma_c}\right). \tag{7}$$

The parameter ξ also denotes the photon number when $\bar{N} = N_0$ is achieved [2]. Moreover, we found that Eq. (5) is further simplified by introducing a new parameter $\tilde{\beta}$ defined as

$$\tilde{\beta} = \frac{\beta}{\xi(1-\beta)+1}. \tag{8}$$

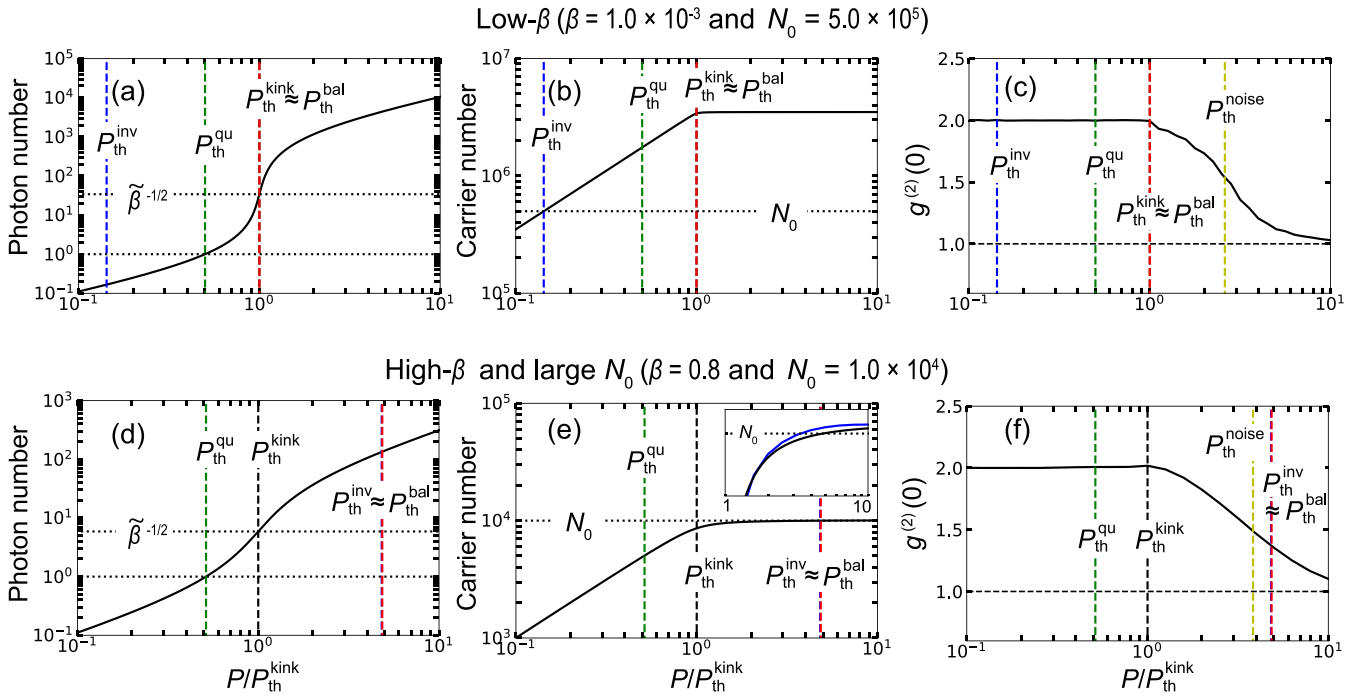

FIG. 1. (a), (d) Steady-state photon $\bar{n}$ and (b), (e) carrier number $\bar{N}$ as a function of pump power normalized by the kink threshold $P_{\rm th}^{\rm kink}$, which are based on the steady-state solutions of the rate equations. (c), (f) Calculated $g^{(2)}(0)$ based on stochastic numerical simulations of the master equation. (a), (b), (c) are plots for low-β lasers with low-Q cavities where $\beta = 10^{-3}$, $1/\gamma_c = 1.0$ ps, $1/\gamma_\parallel = 3.0$ ns, and $N_0 = 5.0 \times 10^5$, thus, $\xi = 0.17$. (d), (e), (f) are for high-β lasers with large-N_0 and high-Q cavities where $\beta = 0.8$, $1/\gamma_c = 50$ ps, $1/\gamma_\parallel = 3.0$ ns, and $N_0 = 1.0 \times 10^4$, thus $\xi = 133$. The blue, green, black, and red vertical dashed lines, respectively, represent the inversion $P_{\rm th}^{\rm inv}$, quantum $P_{\rm th}^{\rm qu}$, kink $P_{\rm th}^{\rm kink}$, and gain-loss balance $P_{\rm th}^{\rm bal}$ thresholds. In the low-β lasers (a), (b), (c), the black and red lines overlap $P_{\rm th}^{\rm kink} \simeq P_{\rm th}^{\rm bal}$, whereas in the high-$\beta$ lasers (d), (e), (f) the blue and red lines overlap $P_{\rm th}^{\rm inv} \simeq P_{\rm th}^{\rm bal}$. The yellow vertical dashed lines in (c), (f) represent the noise threshold $P_{\rm th}^{\rm noise}$ defined and explained in Sec. V. The two horizontal dotted lines in (a), (d) represent the photon number of unity and $\tilde{\beta}^{-1/2}$. The horizontal dotted lines in (b), (c) represent the carrier transparency numbers N_0. The inset in (e) is an enlarged figure and plots the carrier number simulated with the birth-death master equation (blue curve) and with the rate equations (black curve), which shows the blue curve reaches N_0 with a smaller pump power than the black line.

With $\tilde{\beta}$, the steady-state photon number $\bar{n}$ [Eq. (5)] is reduced to

$$\bar{n} = \frac{1}{2\tilde{\beta}}[-(1-\tilde{\beta}P/\gamma_c) + \sqrt{(1-\tilde{\beta}P/\gamma_c)^2 + 4\tilde{\beta}^2 P/\gamma_c}\,], \tag{9}$$

which has the same form as the input-output curve without the carrier transparency number $\xi = 0$ ($N_0 = 0$). The consequence of Eq. (9) is very important because β and N_0 cannot be extracted solely by the fitting of input-output curves. Instead, the fitting of input-output curves gives the parameter $\tilde{\beta}$. We note that $N_0 \simeq 0$ is reasonable for some gas and solid-state lasers [8], which could be modeled as four-level lasers. Meanwhile, $N_0 \simeq 0$ is not realistic in semiconductor lasers.

Now, we briefly discuss the effect of the carrier transparency number N_0 on the photon lifetime and β. As the photon rate equation Eq. (1) indicates, far below the kink threshold, assuming $N \simeq 0$, photon decay rate is effectively enhanced as $\gamma_c \to \gamma_c^{\rm eff} = \gamma_c(1+\xi)$. Actually, this argument is the same as the widely known fact that the effective Q value is limited by carrier absorption. Additionally, N_0 effectively decreases β as $\beta \to \tilde{\beta}$. The clear kink of the pump-input and light-output curve in Fig. 1(a) is due to N_0. Around and above the kink threshold, the effect of N_0 is very complicated and numerical simulations are necessary for each case. Roughly speaking, ξ works as a measure of the effect of the carrier transparency number on lasing properties. When ξ is large, N_0 modifies the behavior of a laser a lot. Namely, a large kink will appear in a pump-input and light-output curve and a relaxation oscillation will have a high oscillation frequency and a large damping rate. Appendix B includes simulations with and without N_0 for low- and high-β lasers.

C. Birth-death master equation

To simulate the photon statistical property of lasers, we employ the birth-death master equation approach that was developed for class-B lasers [7,21,38,39]. The rate equations (1) and (2) are reinterpreted as a birth-death master equation [7,38]:

$$\begin{aligned}\dot{p}_{n,N} = &-\gamma_c[np_{n,N} - (n+1)p_{n+1,N}] \\ &-\beta\gamma_\parallel[(n+1)Np_{n,N} - n(N+1)p_{n-1,N+1}] \\ &-(1-\beta)\gamma_\parallel[Np_{n,N} - (N+1)p_{n,N+1}] \\ &-\beta\gamma_\parallel N_0[np_{n,N} - (n+1)p_{n+1,N-1}] \\ &-P[p_{n,N} - p_{n,N-1}],\end{aligned} \tag{10}$$

which is the equation of motion for the probability $p_{n,N}(t)$ of finding n photons and N carriers in the system at time t. In other words, $p_{n,N}$ is the diagonal part of the density matrix of the system. Since $p_{n,N}$ is the probability, it satisfies the normalization condition $\sum_{n',N'} p_{n',N'} = 1$. All physical observables are calculated as statistical averages. For example, the photon number $\langle n \rangle$ and carrier number $\langle N \rangle$ are calculated as $\langle n \rangle = \sum_{n',N'} n' p_{n',N'}$ and $\langle N \rangle = \sum_{n',N'} N' p_{n',N'}$, respectively. The simulated $\langle n \rangle$ and $\langle N \rangle$ qualitatively give the same results as the mean-field results Eq. (1) and (2).

Strictly speaking, the carrier number N has an upper limit, which is very important in lasers with a few quantum dots. In the atomic picture, the upper limit is the number of emitters. In the many-body electron-hole picture, the upper limit is due to the phase space filling associated with the Pauli blocking [10]. The model used in Ref. [20] is similar to ours, but they considered the upper limit of the carrier number in a few QDs lasers. In our paper, for simplicity, we neglect the upper limit of the carrier number. In particular, in high-β and large-N_0 lasers, the carrier number saturates before reaching the upper-limit. The inclusion of the upper limit of N in the simulation of the birth-death master equation may not be difficult and an interesting direction.

D. Monte Carlo simulation

Although the master equation (10) can be numerically integrated by treating $p_{n,N}$ as a vector, the length of the vector, which is given by $n \times N$, is usually too large for computations. Therefore, we overcome this problem by performing Monte Carlo simulations [12,26,39,40] based on the Gillespie algorithm [39,41,42], which was originally invented for simulating chemical master equations. The main idea of the Gillespie algorithm is to stochastically calculate the time of the next event and determine which event will occur. As we can see from the master equation (10), there are five events in our simulation. We calculate the probability of the five events $a_{\nu\ \{\nu=1,\cdots,5\}}$ at time t as $a_1 = \gamma_c n$, $a_2 = \beta\gamma_\parallel (n+1)N$, $a_3 = (1-\beta)\gamma_\parallel N$, $a_4 = \beta\gamma_\parallel N_0 n$, and $a_5 = P$. In the Gillespie algorithm, the next event takes place at time $t + \tau_j$, where the interval time τ_j is computed as $\tau_j = (1/a_0)\ln(1/r_1)$. Here, r_1 is a uniformly distributed random number ranging from 0–1 and $a_0 = \sum_{\nu=1}^{5} a_\nu$. Then, we determine which event will occur. The index of the next event μ is chosen to satisfy the condition: $\sum_\nu a_\nu^{\mu-1} < a_0 r_2 \leqslant \sum_\nu a_\nu^{\mu}$, where r_2 is another uniformly distributed random number ranging from 0–1. By repeating the above procedure thousands of times, all physical quantities are calculated as statistical averages.

E. Second-order photon correlation

Now we explain the second-order photon correlation function. In time-independent systems, the second-order correlation $g^{(2)}(\tau)$ is defined as

$$g^{(2)}(\tau) \equiv \frac{G^{(2)}(\tau)}{\langle \hat{n} \rangle^2}, \tag{11}$$

where $\langle \hat{n} \rangle$ is the mean photon number and $G^{(2)}(\tau)$ is the non-normalized second-order photon correlation function given by [43,44]

$$\begin{aligned} G^{(2)}(\tau) &\equiv \mathrm{tr}\{\hat{\rho}(0)\hat{a}^\dagger(0)\hat{a}^\dagger(\tau)\hat{a}(\tau)\hat{a}(0)\} \\ &= \mathrm{tr}\{\hat{U}(\tau)\hat{a}\hat{\rho}(0)\hat{a}^\dagger\hat{U}^\dagger(\tau)\hat{a}^\dagger\hat{a}\}. \end{aligned} \tag{12}$$

Here, $\hat{U}(\tau)$ is the Liouvillian time evolution operator from time $t = 0$ to $t = \tau$ and we assume $\hat{a}(0) = \hat{a}$. For the derivation of Eq. (12), we used the relation $\hat{a}(\tau) = \hat{U}^\dagger(\tau)\hat{a}\hat{U}(\tau)$ and the invariance of trace under cyclic permutations. Equation (12) indicates that a single photon detector annihilates one photon at time $t = 0$ as $\hat{\rho}(0) \to \hat{a}\hat{\rho}(0)\hat{a}^\dagger$ and, after the detection, the diagonal part of the density matrix evolves again according to the master equation [Eq. (10)] until the final photon detection measurement at time $t = \tau$. If the single photon annihilation at time $t = 0$ is interpreted as a perturbation that drives the system out of equilibrium as $\hat{\rho}(0) \to \hat{a}\hat{\rho}(0)\hat{a}^\dagger$, the function $g^{(2)}(\tau)$ represents the relaxation process of a perturbed system to a steady state [45]. Therefore, the dynamics of $g^{(2)}(\tau)$ is the quantum counterpart of the relaxation oscillation obtained with the conventional small signal analysis.

For zero delay time $\tau = 0$, the second-order photon correlation function reads

$$g^{(2)}(0) \equiv \frac{\langle \hat{n}(\hat{n}-1) \rangle}{\langle \hat{n} \rangle^2}, \tag{13}$$

which represents photon fluctuation. When $g^{(2)}(0) > 1$, $g^{(2)}(0) = 1$, and $g^{(2)}(0) < 1$, photon statistics are categorized as the super-Poissonian, Poissonian, and sub-Poissonian, respectively. Normally, lasers present the transition from $g^{(0)} = 2$ (thermal) to 1 (Poissonian) with an increase in pump power. We note that the normalized second-order photon correlation function $g^{(2)}(\tau)$ is unchanged by the linear photon losses and finite quantum efficiencies of detectors [46]. The robustness of $g^{(2)}(\tau)$ against linear losses is the major advantage of measuring the second-order photon correlation instead of other photon statistical quantities.

Finally, we comment on the calculation of laser linewidth. Since linewidth is associated to the first-order photon correlation $G^{(1)}(\tau) \equiv \mathrm{tr}\{\hat{\rho}\hat{a}^\dagger(\tau)\hat{a}(0)\}$ and its calculation requires the off-diagonal part of the density matrix that is not captured in the birth-death master equation, linewidth is beyond the scope of this paper.

III. LASING THRESHOLDS

In this section, we discuss the definitions of lasing threshold. Based on the steady-state solutions of the rate equations (5) and (6), in Fig. 1, we plot the steady-state photon $\bar{n}$ and carrier number $\bar{N}$ as a function of the pump power for two cases. The first case [Figs. 1(a)–1(c)] is a low-β laser with a low-Q cavity, which has the parameters $\beta = 10^{-3}$, $N_0 = 5.0 \times 10^5$, $1/\gamma_c = 1.0$ ps, and $1/\gamma_\parallel = 3.0$ ns. These parameters result in $\xi = 0.17$. The second case [Figs. 1(d)–1(f)] is for a high-β laser with a high-Q cavity where $\beta = 0.8$, $1/\gamma_c = 50$ ps, $1/\gamma_\parallel = 3.0$ ns, and $N_0 = 10^4$, thus $\xi = 133$. We also present $g^{(2)}(0)$ in Figs. 1(c) and 1(f) with a stochastic simulation of the master equation.

A. Various definitions of lasing threshold

As discussed in Refs. [2,23] for the first time, there is more than one definition of the lasing threshold. In the following, we review four different definitions of lasing threshold that are plotted as colored vertical dashed lines in Fig. 1.

(i) Kink threshold. First, from the steady-state photon number Eq. (9), we consider a lasing threshold defined as

$$P_{\rm th}^{\rm kink} = \frac{\gamma_c}{\tilde{\beta}} = \gamma_c \frac{\xi(1-\beta)+1}{\beta}. \tag{14}$$

As displayed in Fig. 1, this is the pump power at which the kink of an input-output curve in a log-log scale curve appears, where the photon number is $\tilde{\beta}^{-1/2}$. Thus, we refer to $P_{\rm th}^{\rm kink}$ as the kink threshold, which is easily accessible in measurements. In terms of carriers, the carrier number starts to saturate at the kink threshold, which is the origin of the appearance of the nonlinear buildup of an input-output curve. The kink threshold was introduced by Rice and Carmichael but without the carrier transparency number $N_0 = 0$ [7]. The kink threshold is well defined even in a high-β and a large-N_0 regime.

(ii) Gain-loss balance threshold. Second, we introduce a widely used definition of lasing threshold, which states that the threshold is where the gain is equal to the cavity loss $\beta\gamma_\parallel(\bar{N}-N_0) = \gamma_c$. As explained in Ref. [2], strictly speaking, this balance between gain and loss is achieved with an infinite photon number. Approximating the carrier number $\bar{N}$ [Eq. (6)] as $\bar{N} \simeq P/\gamma_\parallel$, we obtain an approximated gain $\beta\gamma_\parallel(\bar{N}-N_0) \simeq \beta P - \gamma_c\xi \equiv G_{\rm ap}$. With the condition $G_{\rm ap} = \gamma_c$, the gain-loss balance threshold pump power reads

$$P_{\rm th}^{\rm bal} = \gamma_c \frac{1+\xi}{\beta}. \tag{15}$$

As we can easily find, when β and ξ are small, the gain-loss balance threshold almost coincides with the kink threshold $P_{\rm th}^{\rm bal} \simeq P_{\rm th}^{\rm kink}$. Therefore, in conventional low-β lasers with low-Q cavities, this conventional definition of lasing threshold agrees well with the kink of the input-output curves, which leads to the overlap of the red and black vertical dashed line in Figs. 1(a)–1(c). On the other hand, this definition fails when β approaches a unity because the spontaneous emission contribution is neglected, which will be detailed in Sec. III B.

(iii) Inversion threshold. The third lasing threshold is called the inversion threshold and is given by

$$P_{\rm th}^{\rm inv} = \gamma_c \frac{\xi}{\beta}, \tag{16}$$

which represents the pump power at which a population inversion is created. Interestingly, the inversion threshold can be higher than the kink threshold ($P_{\rm th}^{\rm kink} < P_{\rm th}^{\rm inv}$) when β and ξ are sufficiently large, which is an unconventional regime that will be explained later in terms of intensity jump without inversion. When the mean carrier number $\langle N\rangle$ is calculated with the birth-death master equation, $\langle N\rangle$ reaches N_0 with a smaller inversion threshold pump power than $P_{\rm th}^{\rm inv}$ due to the photon-carrier correlation $\langle nN\rangle \neq \langle n\rangle\langle N\rangle$ [7]. In the master equation approach, $P_{\rm th}^{\rm inv}$ represents the pump power where quantum gain $\langle G_0\rangle = \langle (N-N_0)n\rangle/\langle n\rangle$ becomes zero. We explain this point in detail later.

(iv) Quantum threshold. Finally, we explain the quantum threshold proposed in Refs. [2,23], which is defined as the pump power at which the photon number inside the cavity becomes unity. The quantum threshold is expressed as

$$P_{\rm th}^{\rm qu} = \gamma_c \frac{1+\tilde{\beta}}{2\tilde{\beta}} = \frac{1}{2}P_{\rm th}^{\rm kink} + \frac{\gamma_c}{2}. \tag{17}$$

As shown in Fig. 1, the quantum threshold is located at beginning of the nonlinear buildup of input-output curves. The quantum threshold also represents the pump power where the stimulated emission $\beta\gamma_\parallel\bar{n}\bar{N}$ exceeds the spontaneous emission $\beta\gamma_\parallel\bar{N}$.

B. Intensity jump without inversion (lasers without inversion)

We compare the four definitions of lasing threshold in detail by using the plots shown in Fig. 1. Let us start with the low-β laser with a low-Q cavity [see Figs. 1(a)–1(c)]. In this case, the lowest threshold is the inversion threshold, which is much lower than even the quantum threshold. Thus, in conventional low-β lasers with low-Q cavities, a population inversion is created before the photon number inside the cavity reaches unity. Additionally, the gain-loss balance threshold agrees well with the kink threshold. Thus, in low-β low-Q lasers, the widely used definition of lasing threshold works very well: the threshold is where the gain is equal to the photon loss.

On the other hand, when a laser has a high β, high Q, and moderate $N_0(=10^4)$, the results are completely different. Figures 1(d)–1(f) show that the inversion threshold is much higher than the kink threshold. This regime was called lasers without inversion by Yamamoto and Björk, but we name it as intensity jump without inversion to avoid confusion with other lasing without inversion phenomena such as lasing in EIT systems [47,48] and polariton lasers [49–51]. Furthermore, another reason to use the term intensity jump without inversion is because the Poissonian photon statistics $g^{(2)}(0) \simeq 1$ and linewidth narrowing must be confirmed for a claim of lasing.

Moreover, in the intensity jump without inversion regime, the widely used gain-loss balance threshold $P_{\rm th}^{\rm bal}$ fails and it deviates from the kink threshold. To understand the origin of the breakdown of $P_{\rm th}^{\rm bal}$, we define the gain G_0 as

$$G_0 = \beta\gamma_\parallel(\bar{N}-N_0) \tag{18}$$

and the photon increase rate due to the spontaneous emission divided by a mean photon number as

$$S_0 = \beta\gamma_\parallel\bar{N}/\bar{n}. \tag{19}$$

As easily found from the photon rate equations Eq. (1), in a steady state ($\dot{n}=0$),

$$G_0 + S_0 = \gamma_c \tag{20}$$

is satisfied. This indicates that, in a steady state, the photon loss is compensated by G_0 and S_0. In Fig. 2, we plot G_0 and S_0 for the low-β [Fig. 2(a)] and high-β [Fig. 2(b)] lasers, where the parameters are the same as in Fig. 1. Additionally, the dashed curves in Fig. 2 represent the approximated gain

$$G_{\rm ap} = (\beta P - \gamma_c\xi), \tag{21}$$

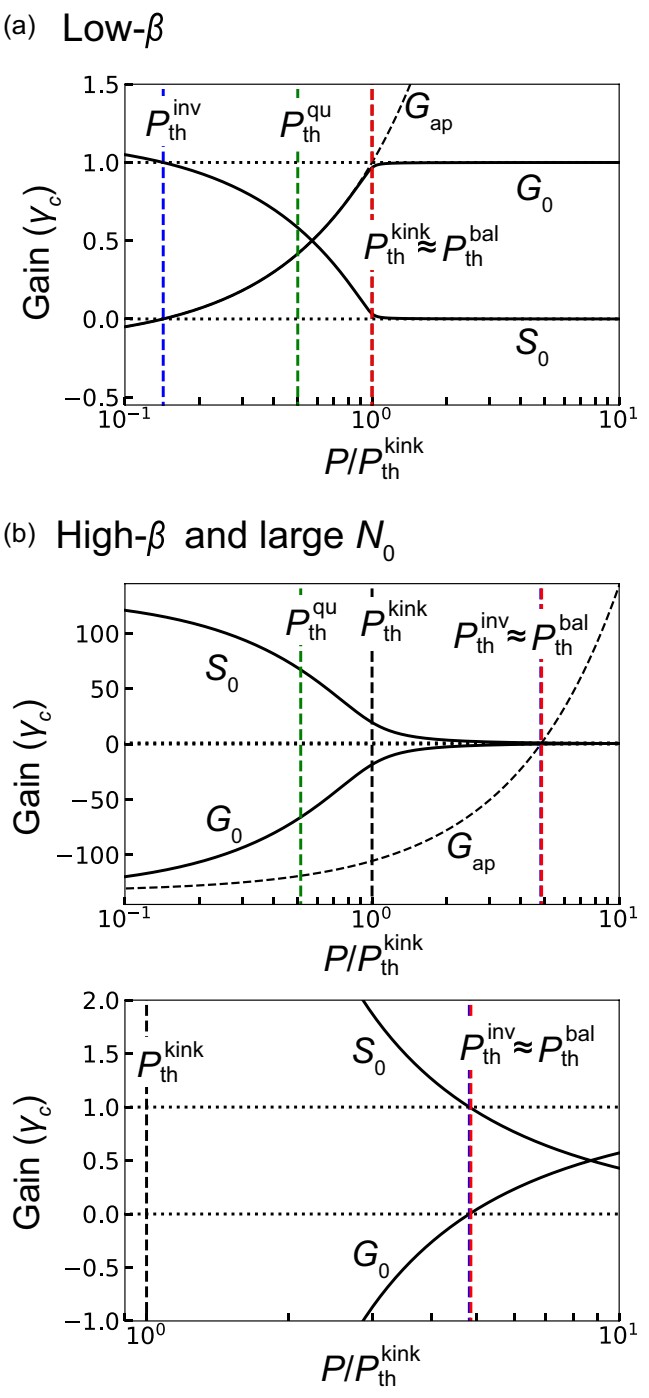

FIG. 2. G_0 and S_0 values defined in Eq. (18) and (19), respectively. The parameters for (a) and (b) are the same as in Figs. 1(a)–1(c) and 1(d)–1(f), respectively. The unit of y axis is the cavity decay rate γ_c. The bottom figure in (b) is the enlarged figure of the top one, which clearly shows the cross of G_0 and S_0. For any pump power $G_0 + S_0 = \gamma_c$ is satisfied. The colored vertical dashed lines represent various thresholds and are defined in Fig. 1.

which was already used in the definition of the gain-loss balance threshold. At the kink threshold of the low-β laser [see Fig. 2(a)], the gain G_0 is dominant and the spontaneous emission S_0 is negligible $G_0 \gg S_0 (\simeq 0)$. Furthermore, the dashed curve in Fig. 2(a) indicates that the approximated gain $G_{\rm ap}$ well extrapolates G_0. Therefore, the gain-loss balance threshold $P_{\rm th}^{\rm bal}$ correctly represents the pump power at which G_0 approximately balances the loss γ_c. In contrast, at the kink threshold of the high-β laser [see Fig. 2(b)], the gain is negative $G_0 < 0$, thus G_0 works as an absorption, while the spontaneous emission contribution S_0 has a large positive value. This indicates that the nonlinear buildup of the light-output is induced by the spontaneous emission S_0, which is a nontrivial regime. Furthermore, the approximated gain $G_{\rm ap}$ fails to extrapolate the gain, which leads to the failure of the gain-loss balance threshold $P_{\rm th}^{\rm bal}$.

Additionally, Fig. 2 clarifies the meaning of the inversion threshold $P_{\rm th}^{\rm inv}$ and the quantum threshold $P_{\rm th}^{\rm qu}$. Even though the mean carrier number $\langle N \rangle$ calculated with the birth-death master equation (10) reaches N_0 below $P_{\rm th}^{\rm inv}$ [see the difference of two lines in the inset of Fig. 1(e)], when we calculate quantum gain as $\langle G_0 \rangle = \langle (N - N_0)n \rangle / \langle n \rangle$ with the master equation, $\langle G_0 \rangle$ almost coincides with the Fig. 2 and crosses zero at $P = P_{\rm th}^{\rm inv}$. Thus, in the master equation calculation, the creation of the population inversion $\langle N \rangle > N_0$ does not accord with the sign change of $\langle G_0 \rangle$. This paradox originates from the fact that the photon-carrier correlation cannot be factorized in the master equation calculation: $\langle Nn \rangle \neq \langle N \rangle \langle n \rangle$. Therefore, strictly speaking, in the birth-death master equation approach, the inversion threshold $P_{\rm th}^{\rm inv}$ represents not the creation of a population inversion but the pump power where the quantum gain $\langle G_0 \rangle$ becomes positive. Second, the quantum threshold $P_{\rm th}^{\rm qu}$ represents the pump power where the stimulated emission $\beta \gamma_\parallel \bar{N} \bar{n}$ becomes equal to the spontaneous emission $\beta \gamma_\parallel \bar{N}$ because the photon number becomes a unity at $P = P_{\rm th}^{\rm qu}$. Furthermore, if ξ is smaller than a unity, $G_0 \simeq S_0$ holds at $P = P_{\rm th}^{\rm qu}$. We should also stress that, in the master equation, the stimulated emission process is present even when $G_0 < 0$. For instance, even if $G_0 = 0$, both the stimulated emission and the absorption processes are present and they give rise to fluctuations, which is very important when photon statistics are concerned.

Finally, we discuss the requirements for the intensity jump without inversion. This regime defined as $P_{\rm th}^{\rm kink} < P_{\rm th}^{\rm inv}$ require the condition $\beta \xi > 1$, which is written as

$$\beta^2 N_0 \left(\frac{\gamma_\parallel}{\gamma_c} \right) > 1. \tag{22}$$

This formula indicates that not only a high β and large N_0 but also the ratio $\gamma_\parallel / \gamma_c$ are crucial for the intensity jump without inversion. The ratio $\gamma_\parallel / \gamma_c$ increases both with increases in the Q value of a cavity and the enhancement of $\gamma_\parallel$ by the Purcell effect as indicated by Eq. (3). On the other hand, if we define the intensity jump without inversion as $P_{\rm th}^{\rm qu} < P_{\rm th}^{\rm inv}$, the required condition is

$$(1 + \beta)(1 - \xi) < 1. \tag{23}$$

This condition is much easier to realize than the former one [Eq. (22)] because $\xi > 1$ is sufficient for the intensity jump without inversion.

C. Photon statistics and thresholds

We discuss the relation between the various thresholds and photon statistics $g^{(2)}(0)$. As Figs. 1(c) and 1(f) show, the

situation is very complicated: both figures exhibit the super-Poissonian photon statistics [$g^{(2)}(0) > 1$] even at high pump powers, but none of the four thresholds can predict the transition of $g^{(2)}(0)$ from the thermal to the Poissonian statistics. In particular, the long-tailed super-Poissonian photon statistics of the low-β laser [Fig. 1(f)] are counterintuitive because the input-output curve has the sharp kink threshold. We argue that these long-tailed super-Poissonian photon statistics result from the fact that the photon decay rate is much larger than that of carriers: $\gamma_c \gg \gamma_\parallel$. We call this region class-B limit. This is in stark contrast to low-β class-A lasers ($\gamma_c < \gamma_\parallel$) that present a sharp transition of the photon statistics from thermal to Poissonian at the kink threshold (see Appendix B). In fact, Druten and Lien have demonstrated that when $\gamma_c \gg \gamma_\parallel$, the photon statistics remain super-Poissonian far above the kink threshold even with a class-B laser with a very low β ($\beta = 10^{-5}$) and $N_0 \simeq 0$ [8,27]. Their argument is that when $\gamma_c \gg \gamma_\parallel$, "the inversion dynamics are too slow to efficiently damp the effects of the quantum-noise source." [8] Another possible interpretation of the supper-Poissonian tail is associated to the saturation of the carrier number and spontaneous emission. As we find from Eq. (6), the saturated carrier number becomes larger with the increase of the ratio $\gamma_c/\gamma_\parallel$. Since the spontaneous emission rate into the cavity per photon is given by $\beta\gamma_\parallel \bar{N}/\bar{n}(= S_0)$, a large ratio $\gamma_c/\gamma_\parallel (\gg 1)$ may give rise to an extra spontaneous emission noise and the super-Poissonian tail above the kink threshold. This interpretation is detailed in Appendix B 1. Furthermore, Chow, Jahnke, and Gies have simulated QD lasers with low-Q cavities and found the super-Poissonian tail [52]. Their interpretation is that lasers become LED-like with the decreases of the photon lifetime. In summary, in class-B lasers, the thermal photon emission remains high even above the kink threshold and previously proposed thresholds do not indicate the inflection point of $g^{(2)}(0)$. In Sec. V, we attempt to propose a possible definition of noise threshold based on the damping time of the relaxation oscillation within a small signal analysis.

Additionally, it is interesting to ask whether or not it is possible to reach $g^{(2)}(0) \simeq 1$ before reaching the inversion threshold $P = P_{\rm th}^{\rm inv}$. Although, in Fig. 1(f), $g^{(2)}(0)$ is only about 1.4 at the pump power $P = P_{\rm th}^{\rm inv}$, in Fig. 12(a) in Appendix B, $g^{(2)}(0) \simeq 1$ is achieved with a much lower pump power than $P_{\rm th}^{\rm inv}$. Therefore, with optimized parameters, it would be possible to obtain the Poissonian photon statistics below the inversion threshold. In Appendix B, we also provide the physical interpretation of this phenomenon.

IV. EXPERIMENT

A. Experimental setup

Here, we describe our experimental setup, which is schematically illustrated in Fig. 3. The nanocavity laser is composed of an InP photonic crystal (PhC) cavity and three buried InGaAsP/InGaAs multiquantum wells (MQWs) [5]. The PhC slab has a two-dimensional (2D) hexagonal lattice with a lattice constant of 424 nm and its thickness is 245 nm. The PhC cavity consists of three missing air holes with two end holes shifted by 106 nm and this is called an L3 cavity. The MQW region with a volume of $0.30 \times 1.25 \times 0.145\ \mu\text{m}^3$ is embedded in the cavity region with the regrowth method [4]. All experiments are carried out at room temperature. The PhC nanocavity laser is pumped with a continuous wave (CW) semiconductor laser operating at 640 nm. The laser outputs from the sample are carried to superconducting single photon detectors (SSPDs) through single-mode optical fibers, which select a single transverse mode. Additionally, a single longitudinal lasing mode is extracted with an interference filter. To measure the second-order photon correlation $g^{(2)}(\tau)$, we employ a conventional Hanbury-brown Twiss (HBT) interferometer. We assume that the resolution time of the SSPDs, which is about 30 ps, is fast enough to measure the second-order photon correlation, which has a typical width of 100 ps.

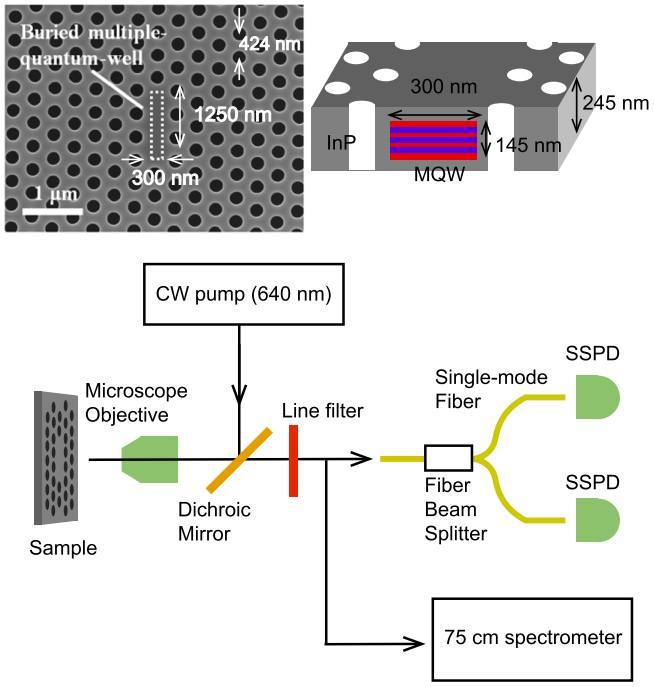

FIG. 3. Scanning electron microscope (SEM) image and structure of a PhC nanocavity laser with an MQW (top). Schematic of experimental setup (bottom).

B. Pump-input and light-output curve

First, in Fig. 4(a), we show the output photon number as a function of the pump input, which is called an pump-input and light-output (input-output) curve. Figure 4(b) shows the linewidth of the emission, which reveals that the linewidth decreases below the spectral resolution of the spectrometer. The kink of the input-output curve and the narrowing of the linewidth displayed in Fig. 4(b) imply a lasing transition. We fit the input-output curve with the steady-state photon number Eq. (9). From the fitting, we find $\tilde{\beta} = 0.019$. The vertical dashed black lines in Fig. 4 show the kink threshold $P_{\rm th}^{\rm kink}$, which corresponds to an excitation light power of 0.127 mW.

Now, we attempt to calculate the conventional spontaneous coupling coefficient β from the measured input-output curve. For this purpose, β is inversely solved from Eq. (7) together

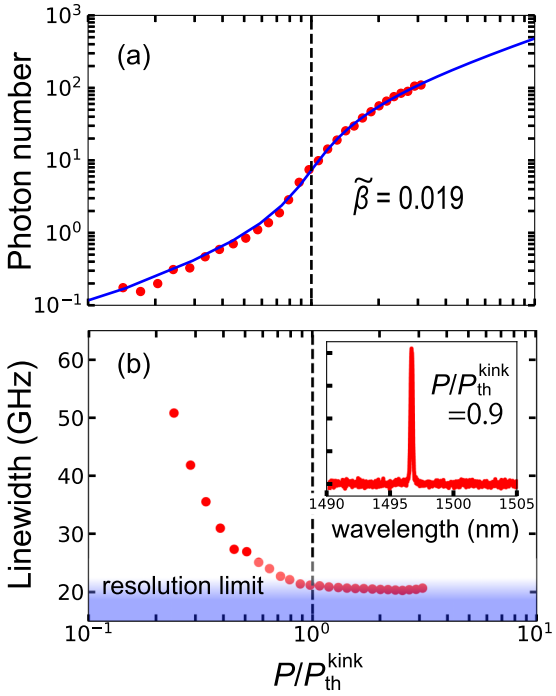

FIG. 4. Measured output photon number (input-output curve) (a) and linewidth (b) as a function of pump power. In (a), the output photon number in the y axis is estimated from the fitting of the measured light output intensity and pump light intensity curve with Eq. (9). The linewidth measurement is limited by the resolution of the spectrometer, which is represented by the blue shaded area. The pump power is normalized by the kink threshold of the input-output curve, which is represented by the vertical dashed lines. The blue solid line in (a) is a fitting with Eq. (9), which gives $\tilde{\beta} = 0.019$. The inset in (b) is the emission spectrum at $P/P_{\rm th}^{\rm kink} = 0.9$.

with Eq. (8) as

$$\beta = \frac{1}{2\tilde{\beta}C}\left[-(1-\tilde{\beta}C) + \sqrt{(1-\tilde{\beta}C)^2 + 4\tilde{\beta}^2 C}\right], \tag{24}$$

where $C = (\gamma_\parallel/\gamma_c)N_0$ and $N_0 \neq 0$. This equation indicates that, to obtain β from $\tilde{\beta}$, we need to know three parameters: γ_c, $\gamma_\parallel$, and N_0. First, the carrier lifetime of III–V QW at room temperature $1/\gamma_\parallel$ is of the order of a few nanoseconds: $1/\gamma_\parallel = 3$–10 ns [53–55]. We performed the time resolved measurement of the carrier decay with a bare QW at room temperatures and the measured carrier lifetime was 4.6 ns (not shown). On the other hand, the photon lifetime γ_c is related to the Q value as $1/\gamma_c = Q\lambda/2\pi c$, where c is the speed of light. We need the Q value of the L3 InP PhC cavity without carrier absorption in the MQW, but unfortunately, experimentally we can only measure the decreased Q value with the carrier absorption, which is typically a few thousands: $Q_{\rm abs} = 1000 \sim 7000$ [5]. Finally, the carrier transparency number N_0 is given by $N_0 = n_{\rm 3D}V_{\rm act}$, where $n_{\rm 3D} \sim 10^{18}$ cm^{-3} is the 3D carrier transparency density [5] and $V_{\rm act}$ is the active mode volume. When we take the volume of the three quantum wells buried in the L3 cavity into account, we obtain $V_{\rm act} = 7.4 \times 10^{-15}$ cm^3, which leads to $N_0 = n_{\rm 3D}V_{\rm act} \sim 6.0 \times 10^3$. Meanwhile, if we use the 2D carrier transparency density of a quantum well $n_{\rm 2D} \sim 1.5 \times 10^{12}$ cm^{-2} [56], we estimate the carrier transparency number as $N_0 = n_{\rm 2D}S_{\rm act} \sim 1.7 \times 10^4$, where $S_{\rm act} = 1.1 \times 10^{-8}$ cm^2 are the areas of the three quantum wells. To summarize, the carrier transparency number is estimated to be $N_0 = 6.0 \times 10^3 \sim 1.7 \times 10^4$.

As we see, these are very crude estimations, and the information obtained from the light-input and light-output curve is very limited. Therefore, additional information is required if we are to more precisely determine the parameters. For this purpose, in Sec. IV C, we make use of the delay-dependent second-order correlation function.

C. Second-order photon correlation

We discuss not only the second-order photon correlation function at a zero time delay $g^{(2)}(0)$ but also the delay-dependent function $g^{(2)}(\tau)$. The measurement of $g^{(2)}(0)$ is commonly performed to confirm a lasing transition, whereas the time delay dependence of $g^{(2)}(\tau)$ is rarely studied. We carried out systemic measurements of $g^{(2)}(\tau)$ and show that the delay dependence of $g^{(2)}(\tau)$ is useful for determining such parameters as β and N_0.

We present measured $g^{(2)}(\tau)$ values for three different pump powers in Fig. 5(d). First, we find that the bunching behavior of $g^{(2)}(\tau)$ gradually disappears as the pump power increases. Figure 5(a) shows measured $g^{(2)}(0)$ as a function of pump power, which presents a gradual transition from thermal [$g^{(2)}(0) = 2$] to Poissonian [$g^{(2)}(0) = 1$] photon statistics. Second, let us focus on the time delay dependence of the measured $g^{(2)}(\tau)$. Clearly, $g^{(2)}(\tau)$ for $P/P_{\rm th}^{\rm kink} = 2.7$ [see Fig. 5(d)] clearly shows damped oscillatory behavior, which can be fitted as

$$g^{(2)}(\tau) = 1 + [g^{(2)}(0) - 1]e^{-\gamma_r|\tau|}\cos(\omega_r|\tau| + \phi). \tag{25}$$

The measured oscillation frequencies ω_r and damping times $1/\gamma_r$ are plotted as red dots in Figs. 5(b) and 5(c), respectively. As already mentioned in Sec. II E, a single photon annihilation drives the system out of equilibrium as $\hat{\rho} \to \hat{a}\hat{\rho}\hat{a}^\dagger$ and the perturbed system relaxes again into a steady state [45]. Thus, the dynamics of the second-order photon correlation $g^{(2)}(\tau)$ represent the relaxation process. We find that the oscillation ω_r becomes faster with increases in pump power [see Fig. 5(b)], whereas the maximum damping time $1/\gamma_r \sim 0.25$ ns is identified around $P/P_{\rm th}^{\rm kink} \sim 3$ [see Fig. 5(c)]. This maximum damping time is used later in the context of the noise threshold. Since this damped oscillatory behavior of the second-order photon correlation is analogous to the relaxation oscillation commonly observed in class-B lasers, the oscillation frequency and the damping time could be approximately calculated with the conventional small signal analysis. In a small signal analysis, the relaxation oscillation is analyzed with the linearization of a small fluctuation around a steady state, which provides analytical formulas of the relaxation oscillation frequency ω_r and damping rate γ_r [8,25]:

$$\omega_{\rm ro} = \sqrt{\beta\gamma_\parallel\gamma_c(\bar{n}-\xi) - \frac{1}{4}\left\{-\gamma_\parallel(1+\beta\bar{n}) + \frac{\gamma_c(1+\xi)}{1+\bar{n}}\right\}^2} \tag{26}$$

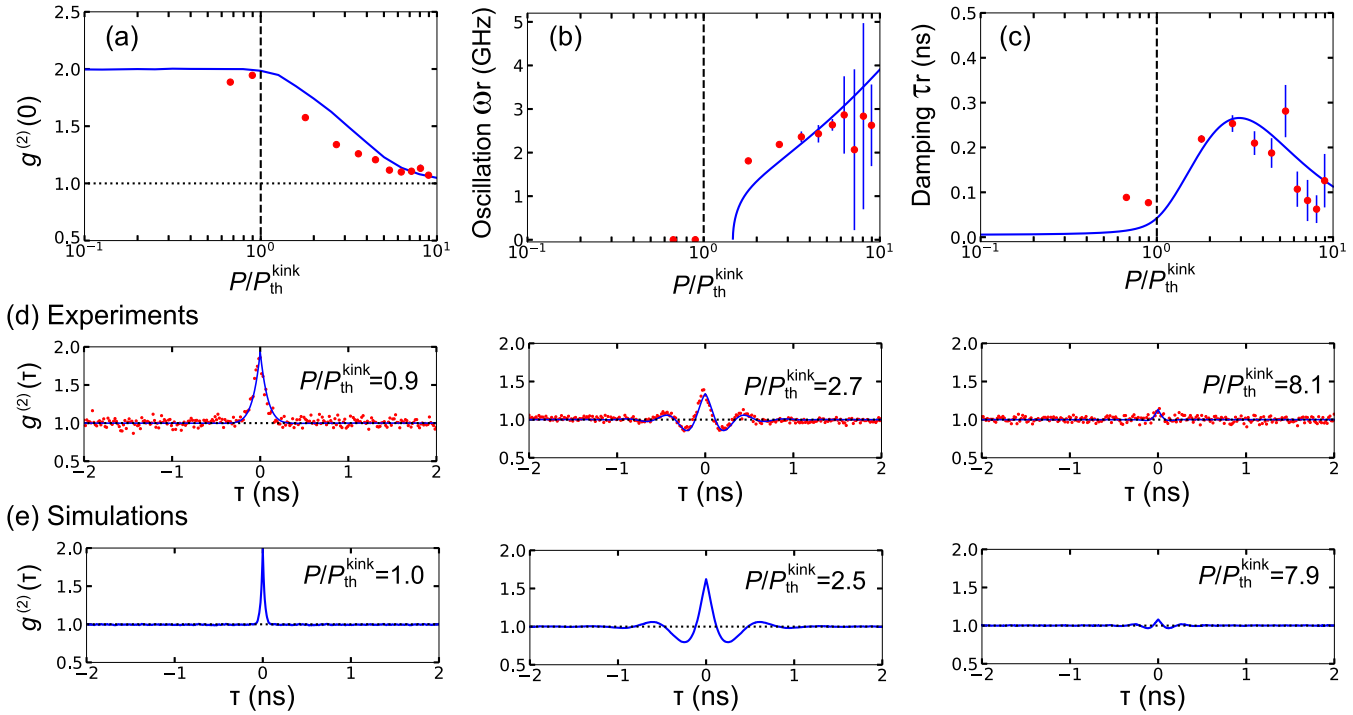

FIG. 5. Second-order photon correlation function $g^{(2)}(\tau)$ measurements performed with a Hanbury Brown-Twiss (HBT) interferometer and superconducting single photon detectors (SSPDs). $g^{(2)}(0)$ (a), the oscillation frequency ω_r, (b) and the damping time $1/\gamma_r$ (c) of $g^{(2)}(\tau)$ are shown as a function of the pump power normalized by the kink threshold. The blue solid lines (a) and (b), (c) are the results of a stochastic simulation of the birth-death master equation and the small signal analysis, respectively. For these simulations and plots, $1/\gamma_c = 25$ ps, $1/\gamma_\parallel = 4.5$ ns, $\beta = 0.16$, and $N_0 = 10000$ are used. These parameters lead to $\xi = 8.7$. Examples of the measured (d) and simulated (e) second-order photon correlation functions.

and

$$\gamma_{ro} = \frac{1}{2}\left\{\gamma_\parallel(1+\beta\bar{n}) + \frac{\gamma_c(1+\xi)}{1+\bar{n}}\right\}. \tag{27}$$

The small signal analysis is explained in detail in Appendix A. Strictly speaking, the linearization procedure is not applicable at the lasing threshold because of the enhanced fluctuations associated and the small number of photons [38]. This implies that we should extract ω_r and γ_r from the simulated $g^{(2)}(\tau)$ based on the master equation. However, since the Monte Carlo simulation of $g^{(2)}$ requires a lot of computation time, we do not employ this method. In fact, it is known that even around the lasing threshold, ω_r and γ_r given by the small signal analysis approximately agree with those based on the master equation [20,23] [see also Fig. 7(d)].

Figure 6 shows $g^{(2)}(0)$, the oscillation frequency ω_r, and the damping time γ_r of $g^{(2)}(\tau)$ for various combinations of β and N_0 that satisfy the same input-output curve. While $g^{(2)}(0)$ is calculated with a stochastic simulation of the master equation, ω_r and γ_r are based on the small signal analysis Eq. (26) and (27). In Fig. 6, the photon and carrier lifetimes are fixed as $1/\gamma_c = 25$ ps and $1/\gamma_\parallel = 4.5$ ns, respectively. As Figs. 6(c) and 6(d) clearly show, ω_r and γ_r are very sensitive to the β and N_0 values in contrast to $g^{(2)}(0)$ that does not vary greatly when the β and N_0 values are changed [see Fig. 6(b)]. Comparing the plotted ω_r and γ_r with the experiments, we estimate the carrier transparency number and the spontaneous coupling coefficient as $N \sim 10000$ and $\beta \sim 0.16$, respectively, which leads to $\xi \sim 8.7$. Of course, since they also depend on the photon $1/\gamma_c$ and carrier $1/\gamma_\parallel$ lifetimes, we need to repeat the same plots as Fig. 6 for various $1/\gamma_c$ and $1/\gamma_\parallel$ values. In fact, after repeating these plots, we found that $1/\gamma_c \sim 25$ ps and $1/\gamma_\parallel \sim 4.5$ ns is one of the best combinations for reproducing the measured results. We note that these parameters agree with the crude estimations obtained in the previous subsection. For the Q value, since the photon decay rate is effectively enhanced as $\gamma_c^{\text{eff}} = (1+\xi)\gamma_c$, the photon lifetime with the carrier absorption is about 2.6 ps and the corresponding Q value with absorption becomes $Q_{\text{abs}} \sim 3.2 \times 10^3$, which agrees well with the previously measured Q value [5].

Finally, we comment on the usefulness of a delay-dependent $g^{(2)}(\tau)$ measurement from a technical standpoint. The oscillation frequency ω_r and the damping rate γ_r of $g^{(2)}(\tau)$ could be obtained with turn-on delay measurements. However, since a step-function-like pump pulse is necessary, whose modulation time must be faster than the oscillation frequency and the damping time, turn-on delay measurements are not always easy to perform. Instead, a delay-dependent $g^{(2)}(\tau)$ measurement can be performed under continuous wave operation without any pump modulation.

D. Lasing thresholds

Here, we discuss the four thresholds introduced in Sec. III with respect to a measured buried MQW PhC laser. Based on the estimated parameters $1/\gamma_c = 25$ ps, $1/\gamma_\parallel = 4.5$ ns, $N_0 = 10000$, and $\beta = 0.16$, we show the four thresholds in Fig. 7 and 8 as colored vertical dashed lines. Even though the values

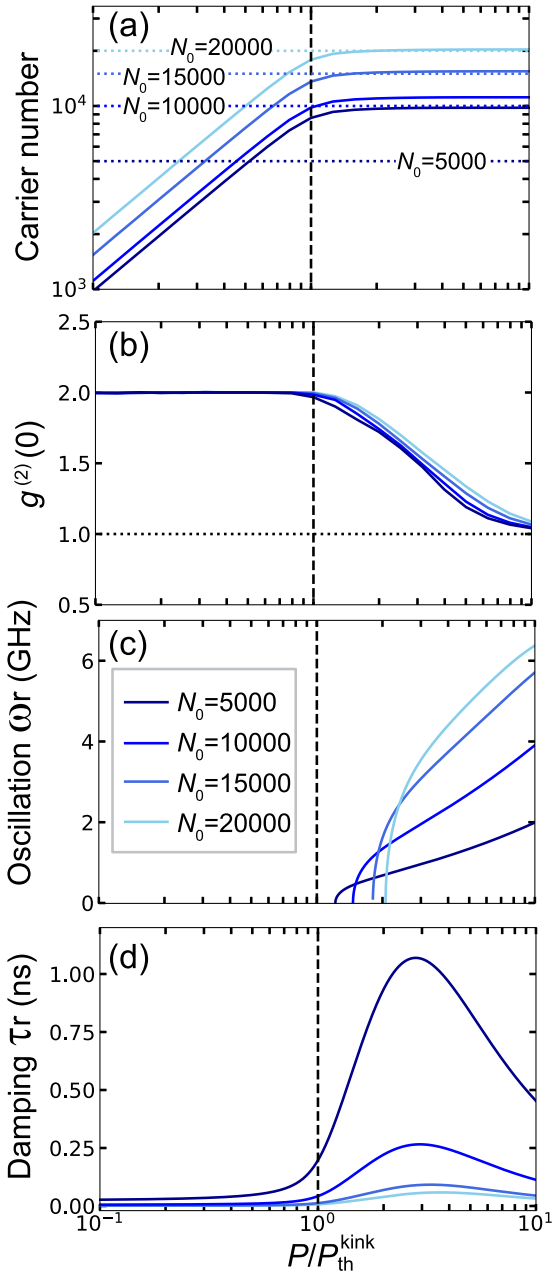

FIG. 6. Fixing $1/\gamma_c = 25$ ps, $1/\gamma_\parallel = 4.5$ ns, and $\tilde{\beta} = 0.019$, we plot (a) the steady-state carrier number, (b) $g^{(2)}(0)$, (c) the oscillation frequency ω_r, and (d) the damping rate γ_r of $g^{(2)}(\tau)$ for four different combinations of N_0 and β. The colored lines represent $N = 5000$ ($\beta = 0.04$), 10000 (0.16), 15000 (0.39), and 20000 (0.54), which respectively correspond to $\xi = 1.0$, 8.7, 33, and 60. While (a) and (b) are based on a stochastic simulation of the master equation, (c) and (d) are plotted with the analytical solution of a small signal analysis.

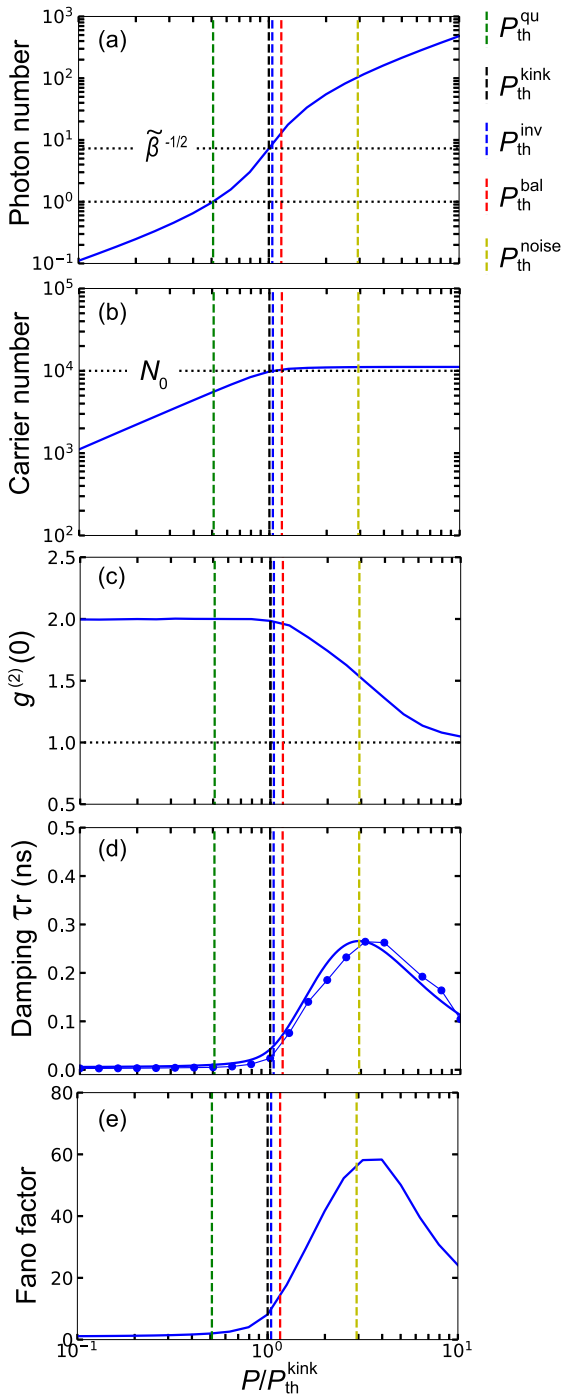

FIG. 7. (a) Simulated input-output curve and (b) carrier number, (c) $g^{(2)}(0)$, (d) damping time γ_r of $g^{(2)}(\tau)$, and (e) the Fano factor for $1/\gamma_c = 25$ ps, $1/\gamma_\parallel = 4.5$ ns, $\beta = 0.16$, and $N_0 = 10000$. These parameters are the same as those used in Fig. 5. The simulations are based on the birth-death master equation. The blue line in (b) is the damping time of the relaxation oscillation with the small signal analysis Eq. (27), whereas the blue filled circle is based on the direct fitting of simulated $g^{(2)}(\tau)$. The blue, green, black, and red vertical dashed lines, respectively, represent the inversion $P_{\rm th}^{\rm inv}$, quantum $P_{\rm th}^{\rm qu}$, kink $P_{\rm th}^{\rm kink}$, and gain-loss balance $P_{\rm th}^{\rm bal}$ thresholds. The yellow vertical dashed line is the noise threshold $P_{\rm th}^{\rm noise}$ defined in Eq. (30). The two horizontal dotted lines in (a) represent photon numbers of unity and $\tilde{\beta}^{-1/2}$. The horizontal dotted line in (b) represents the carrier transparency number $N_0 = 10000$.

of these thresholds contain errors due to the uncertainties of the estimations of parameters, these errors do not greatly affect the following discussion. Figure 7 indicates that the gain-loss balance threshold (the red vertical dashed line) is close to the kink threshold (the black vertical dashed line) $P_{\rm th}^{\rm bal} \lesssim P_{\rm th}^{\rm kink}$. Thus, it may appear that our buried MQW PhC laser can be categorized as a conventional laser, but this is not

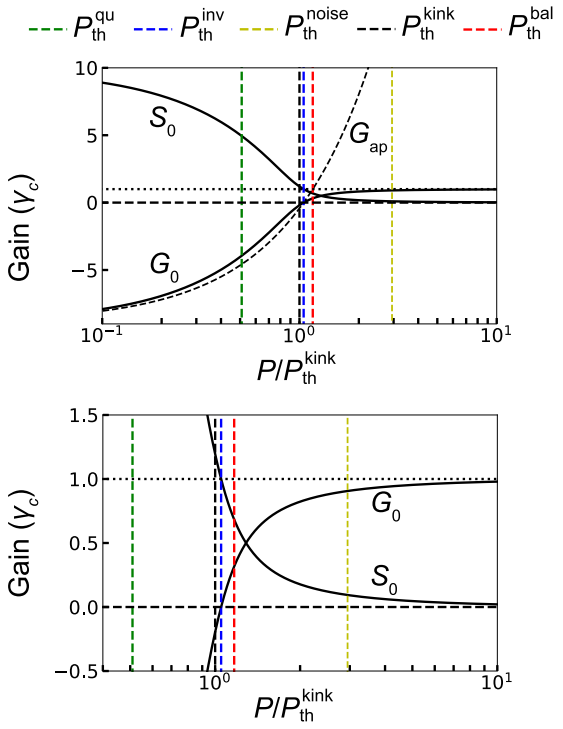

FIG. 8. G_0 and S_0 values are plotted based on the parameters used in Fig. 7. G_0 and S_0 are defined respectively in Eq. (18) and (19). The definition of the colored vertical dashed lines is the same as in Fig. 7.

true with respect to the inversion threshold. We find that the inversion threshold P_{th}^{inv} is larger than the quantum threshold ($P_{th}^{qu} < P_{th}^{inv}$) and, additionally, P_{th}^{inv} is very close to the kink threshold ($P_{th}^{kink} \simeq P_{th}^{inv}$). Recalling that the inversion threshold is much lower than the quantum threshold in conventional low-β lasers [see Fig. 1(a)], we notice that the threshold behavior of our laser is unconventional. With the estimated parameters, Fig. 8 plots the values of G_0 and S_0 defined as Eq. (18) and (19), respectively. This figure clearly shows that the spontaneous emission S_0 dominates over the gain G_0 at the kink threshold. Furthermore, since G_{ap} does not extrapolate G_0 well (see the dashed curve in the top figure of Fig. 8), we argue that the gain-loss balance threshold fails in our laser. In Fig. 7(c), the Poissonian light emission $g^{(2)}(0) \simeq 1$ is achieved above the inversion threshold $P = P_{th}^{inv}$, which is the same as conventional lasers. Further increases of β, N_0, and the photon lifetime will be interesting direction to achieve the more interesting region where Poissonian light is emitted below the inversion threshold. In any case, we could argue that our laser exhibits an unconventional threshold behavior associated with a high β and large N_0 and may fall within the intensity jump without inversion regime.

V. NOISE THRESHOLD

Here, we focus on photon statistics represented by $g^{(2)}(0)$. As we have already discussed, no definition of lasing threshold predicts the transition of photon statistics from the thermal [$g^{(2)}(0) = 2$] to the Poissonian [$g^{(2)}(0) = 1$]. The inflection point of $g^{(2)}(0)(\sim \pi/2 \sim 1.5)$ [57] is located above all the four thresholds, which is about three times higher than the kink threshold. Furthermore, $g^{(2)}(0) = 1$ is achieved at a pump power that is ten times higher than the kink threshold. In fact, as already discussed in Sec. III C, the measured long-tailed bunching of $g^{(2)}(0)$ is the typical photon statistics of lasers in the class-B limit $\gamma_c/\gamma_\parallel \gg 1$: the slow damping relaxation oscillation provides excess noise. Since we obtain $\gamma_c/\gamma_\parallel = 180(\gg 1)$ with the estimated parameters, our laser is evidently classified as a laser within the class-B limit.

Finally, we propose a possible definition for noise threshold. The main idea is that the maximum damping time of the relaxation oscillation [see the τ_r peak in Fig. 5(c)] could be interpreted as the noise threshold at which the thermal to Poissonian transition of $g^{(2)}(0)$ appears (noise threshold). Although this is simply an empirical idea and has not yet been proved rigorously, we can intuitively illustrate it as follows. Since the damping time τ_r characterizes the lifetime of a fluctuation, a longer τ_r would lead to a larger amount of noise due to noise accumulation. Recalling the noise enhancement around the critical points of phase transitions, the maximum value of τ_r would represent both the maximum noise and noise threshold. Furthermore, the enhanced damping time at the noise threshold might be interpreted as the critical slowing down of the amplitude mode in terms of the laser-phase transition analogy [58,59]. Within the small signal analysis, from Eq. (27), when the photon number is

$$n_d = \sqrt{\frac{\gamma_c(1+\xi)}{\beta\gamma_\parallel}} - 1, \tag{28}$$

τ_r reaches its maximum (γ_r is minimum)

$$\tau_{r,\max} = \frac{1}{(1-\beta)\gamma_\parallel/2 + \sqrt{\beta\gamma_c\gamma_\parallel(1+\xi)}}. \tag{29}$$

From the steady-state solutions of the rate equations, the pump power when $\bar{n} = n_d$ is easily calculated as

$$P_{th}^{noise} = \frac{\gamma_c}{\beta}\left[\frac{n_d}{1+n_d}(1+\xi)(1+\beta n_d) - \xi\beta n_d\right], \tag{30}$$

at which point the transition of the photon statistics from thermal to Poissonian will occur $g^{(2)}(0) \sim 1.5$. As Figs. 5 and 7 show, both the experiment and the simulation result in $g^{(2)}(0) \sim 1.5$ where the damping time of the relaxation oscillation becomes maximum. Additionally, in Fig. 7(e) we show the Fano factor defined as

$$F \equiv \frac{(\Delta n)^2}{\langle\hat{n}\rangle} = 1 + \langle\hat{n}\rangle[g^{(2)}(0) - 1], \tag{31}$$

which represents the photon number variance divided by the mean photon number. The peak of the Fano factor at around the noise threshold P_{th}^{noise} illustrates the enhancement of the photon noise at the maximum damping time of the relaxation oscillation. We found that the noise threshold Eq. (30) characterizes the inflection point of $g^{(2)}(0)$ in a wide range of parameters in class-B lasers [see Figs. 1(c)–1(f) and Appendix B]. However, we note that Eq. (30) cannot be used in class-A lasers because the small signal analysis fails, but the noise threshold will be still the pump power at which the damping time of $g^{(2)}(\tau)$ is at its maximum (see Appendix. B). The lasing thresholds and photon statistics of high-β lasers in the class-A regime will be the subjects of future investigations.

The interesting application of the noise threshold is to the thresholdless lasers ($\beta = 1$). As is well known, input-output curves become thresholdless when β is unity, but $g^{(2)}(0)$ provides a thresholdlike transition if the lasers are class B. Even in these class-B thresholdless lasers, the damping time of the relaxation oscillation exhibits a peak and the noise threshold Eq. (30) can predict the noise threshold of $g^{(2)}(0)$ [for example, see Fig. 11(b) and Fig. 12(b) in Appendix B].

VI. CONCLUSION

We have investigated the lasing thresholds and photon statistics of buried multiple quantum well (MQW) photonic crystal (PhC) nanocavity lasers. Since our buried MQW PhC has a high spontaneous emission coupling coefficient β and a large carrier transparency number N_0, the definitions of lasing thresholds and photon statistics become nontrivial. For an analysis of lasing thresholds, we need to estimate physical parameters such as β and N_0. Together with the fitting of an input-output curve, we used delay-dependent second-order photon correlations $g^{(2)}(\tau)$ that provide information on the dynamical properties of lasers. Finally, we estimated that our buried MQW PhC laser had $N_0 \sim 10^4$ and $\beta \sim 0.16$, which imply that a population inversion is created around the kink threshold of the input-output curve. Since in conventional low-β lasers, the population inversion is formed far below the kink threshold, our laser is operating in an unconventional regime and very close to the lasers without inversion (intensity jump without inversion) regime proposed by Yamamoto and Björk.

We also discussed the photon statistics of the buried MQW PhC lasers and the noise threshold. The measured $g^{(2)}(0)$ showed that the super-Poissonian photon statistics remained even far above the kink threshold and were found to be the characteristic photon statistics of lasers in the class-B limit, in which region the excess noise is driven by a slow damping relaxation oscillation. Since previously proposed definitions of lasing threshold cannot predict the noise threshold of $g^{(2)}(0)$ in class-B lasers, we proposed a possible definition of the noise threshold that is defined as the pump power where the damping time of the relaxation oscillation reaches its maximum. Our proposed noise threshold explains the measured photon statistical behaviors.

We believe that our results will trigger a reconsideration of the definitions of thresholds and photon statistics of lasers with a high β and large N_0 and cast light on the physics of cavity-QED lasers.

Note added in proof. Recently we became aware of a paper with a similar motivation [60].

ACKNOWLEDGMENTS

We thank S. Kita, K. Takata, and T. Kakitsuka for helpful discussions.

APPENDIX A: SMALL SIGNAL ANALYSIS

In this Appendix, we analyze the relaxation oscillation with a conventional linearization method called a small signal analysis [8,14,20,25,28,32]. Although the linearization is inapplicable to the lasing operation near the threshold in a strict sense, a small signal analysis is a very convenient and intuitive method and it gives approximately the same results as the birth-death master equation of class-B lasers. First, we write the photon and carrier numbers as $n = \bar{n} + \delta n$ and $N = \bar{N} + \delta N$, respectively, and substitute them into the rate equations (1) and (2). Here, $\bar{n}$ and $\bar{N}$ are the steady-state photon and carrier numbers given in Eqs. (5) and (6), respectively, whereas δn and δN, respectively, are photon and carrier fluctuations around the steady states. Taking only the linear terms of the fluctuations, the equations of motion of δn and δN follow

$$\frac{d}{dt}\begin{pmatrix}\delta n\\ \delta N\end{pmatrix} = \boldsymbol{M}\begin{pmatrix}\delta n\\ \delta N\end{pmatrix}, \tag{A1}$$

where the matrix $\boldsymbol{M}$ reads

$$\boldsymbol{M} = \begin{pmatrix}-\gamma_c + \beta\gamma_\parallel(\bar{N} - N_0) & \beta\gamma_\parallel(1+\bar{n})\\ -\beta\gamma_\parallel(\bar{N} - N_0) & -\gamma_\parallel(1+\beta\bar{n})\end{pmatrix}. \tag{A2}$$

From the real and imaginary parts of the eigenvalues of the matrix in Eq. (A2), the relaxation oscillation frequency $\omega_{\rm ro}$ and the damping rate $\gamma_{\rm ro}$ are, respectively, obtained as

$$\omega_{\rm ro} = \left[\beta\gamma_\parallel\gamma_c\bar{n} - \beta^2\gamma_\parallel^2 N_0 - \frac{1}{4}\left(-\gamma_\parallel(1+\beta\bar{n}) + \frac{\gamma_c + \beta\gamma_\parallel N_0}{1+\bar{n}}\right)^2\right]^{\frac{1}{2}} \tag{A3}$$

and

$$\gamma_{\rm ro} = \frac{1}{2}\left\{\gamma_\parallel(1+\beta\bar{n}) + \frac{\gamma_c + \beta\gamma_\parallel N_0}{1+\bar{n}}\right\}, \tag{A4}$$

where $\bar{N}$ is eliminated with Eq. (6) and $\bar{n}$ is given by Eq. (5). Rewriting N_0 with ξ, we can obtain Eqs. (26) and (27) in the main text. Using $\omega_{\rm ro}$ and $\gamma_{\rm ro}$, within the framework of the small signal analysis, the decay process of the small fluctuation of photons $\delta n(t)$ is approximated as

$$\delta n(t) \simeq \delta n(0) e^{-\gamma_{\rm ro} t}\cos(\omega_{\rm ro} t + \phi). \tag{A5}$$

Interestingly, the small signal analysis qualitatively well reproduces the oscillation frequency and the damping time of the second-order photon correlation function $g^{(2)}(\tau)$ that can be simulated based on the birth-death master equation. This is because, as discussed in the main text, $g^{(2)}(\tau)$ also represents the relaxation process of the system driven by a single photon annihilation. The relation between $g^{(2)}(\tau)$ and $\delta n(\tau)$ could also be understood in the framework of Onsager's regression hypothesis, which states that the equilibrium correlation functions follow the same equations of motion as those of the nonequilibrium deviation $\delta n(t)$. With this assumption, the correlation functions satisfy [61]

$$\frac{d}{dt}\begin{pmatrix}\langle\Delta n(0)\Delta n(t)\rangle\\ \langle\Delta N(0)\Delta n(t)\rangle\end{pmatrix} = \boldsymbol{M}\begin{pmatrix}\langle\Delta n(0)\Delta n(t)\rangle\\ \langle\Delta N(0)\Delta n(t)\rangle\end{pmatrix}, \tag{A6}$$

where $\boldsymbol{M}$ is the same matrix as Eq. (A2). Thus, $g^{(2)}(\tau)$ can be approximated as

$$g^{(2)}(\tau) = 1 + \frac{\langle \Delta n(0)\Delta n(\tau)\rangle}{\bar{n}^2} \simeq 1 + \frac{\Delta n^2}{\bar{n}^2} e^{-\gamma_{\rm ro}\tau}\cos(\omega_{\rm ro}\tau + \phi), \tag{A7}$$

where $\Delta n^2 = \langle \Delta n(0)\Delta n(0)\rangle$. The above equation indicates that the oscillation frequency and the decay rate of the second-order correlation are approximated, respectively, as $\omega_{\rm ro}$ and $\omega_{\rm ro}$, which are given in Eqs. (A3) and (A4).

APPENDIX B: SIMULATIONS WITH VARIOUS PARAMETERS

Here, we perform simulations with a wide range of parameters. Our objective is not to cover all different parameter regimes but to support the arguments in the main text. Our main purposes are to (i) show the simulations of class-A lasers and to (ii) confirm the validity of the noise threshold introduced in Sec. V.

We note that in the class-A limit $\gamma_c/\gamma_\parallel \ll 1$ without a carrier transparency number ($N_0 = 0$), the adiabatic elimination of the carrier degree of freedom may allow us to obtain the master equation only of photons. This photon master equation could be analytically solved by the detailed balance condition and we may obtain an analytical photon distribution as [48,62]

$$p_n = \frac{(P/\gamma_c)^n \Gamma(1/\beta)}{{}_1F_1(1;1/\beta;P/\gamma_c)\Gamma(n+1/\beta)}, \tag{B1}$$

where ${}_1F_1(a;b;z)$ is the confluent hypergeometric function and $\Gamma(x)$ is the Gamma function. The details of this approach will be discussed elsewhere. Instead, in this Appendix, we directly simulate the birth-death master equation (10).

1. Low-β lasers

First, we simulate low-β lasers ($\beta = 0.001$) without a carrier transparency number ($N_0 = 0$) in Fig. 9, where Fig. 9(a) and 9(b) are simulations, respectively, for class-A ($\gamma_c/\gamma_\parallel = 0.1$) and class-B ($\gamma_c/\gamma_\parallel = 10^3$) parameters. For Fig. 9(a), $1/\gamma_c = 1$ ns, $1/\gamma_\parallel = 0.1$ ns, $\beta = 0.001$, and $N_0 = 0$ are used. For Fig. 9(b), $1/\gamma_c = 1$ ps, $1/\gamma_\parallel = 1$ ns, $\beta = 0.001$, and $N_0 = 0$ are used. As we briefly mentioned in Sec. III B, the zero carrier transparency number is impossible with an ensemble of two-level atoms and unrealistic in conventional semiconductor lasers. However, $N_0 \simeq 0$ is, in principle, possible for example with an ensemble of four-level atoms. In fact, it is known that, in some gas and solid-state lasers [8], the approximation $N_0 \simeq 0$ is reasonable. The second-order photon correlations at a zero delay in Fig. 9 indicate the sharp transition of photon statistics from thermal $g^2(0) = 2$ to Poissonian $g^2(0) = 1$ at the kink threshold $P = P_{\rm th}^{\rm kink}$ for the class-A laser, whereas, for the class-B laser, the tail of super-Poissonian photon statistics [$g^2(0) > 1$] is present above the kink threshold. In the main text, we have already discussed this long-tailed super-Poissonian photon statistics. Figure 9 clarifies that the super-Poissonian tail is associated to the ratio $\gamma_c/\gamma_\parallel$. Comparing the carrier numbers in Fig. 9(a) and 9(b), we find a very large difference. The saturated carrier number

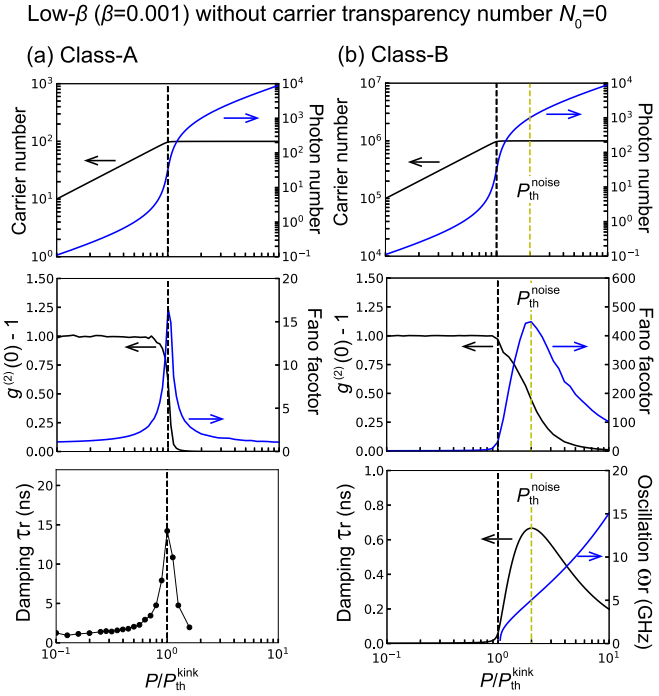

FIG. 9. Simulations for low-β ($\beta = 0.001$) (a) class-A and (b) class-B lasers without a carrier transparency number ($N_0 = 0$). Top figures: carrier number $\bar{N}$ (black line) and photon $\bar{n}$ (blue line). Middle figures: $g^{(2)}(0)$ (black line) and the Fano factor (blue line). Bottom figures: the damping time (black line or filled circles) and oscillation frequency of $g^{(2)}(\tau)$ (blue line). In the bottom figures, the black line is the result of the small signal analysis [Eq. (27)], while the black filled circles are obtained by the fitting of simulated $g^{(2)}(\tau)$. The black and yellow vertical dashed lines respectively represent the kink $P_{\rm th}^{\rm kink}$ and noise $P_{\rm th}^{\rm noise}$ thresholds. The lifetimes are $1/\gamma_c = 1$ ns, $1/\gamma_\parallel = 0.1$ ns for (a), while $1/\gamma_c = 1$ ps, $1/\gamma_\parallel = 1$ ns for (b).

in Fig. 9(a) is just around 100, while the saturated carrier number in Fig. 9(b) is around 10^6. On the other hand, there is no difference between the two pump-input and light-output curves in Figs. 9(a) and 9(b), whose shapes are determined by $\tilde{\beta}$. Therefore, even above the kink threshold, the spontaneous emission rate into the cavity per photon $\beta\gamma_\parallel\bar{N}/\bar{n}(= S_0)$ is much larger in Fig. 9(b) than in Fig. 9(a). Therefore, the supper-Poissonian tail of $g^{(2)}(0)$ in Fig. 9(b) may originate from the strong spontaneous emission noise associated to the large carrier number above the kink threshold. Now, we discuss the damping times of the second-order correlations $g^{(2)}(\tau)$ and the noise threshold. For the class-B laser, the solid line in the bottom figure of Fig. 9(b) is the small signal analysis result given by Eq. (27). Meanwhile, for the class-A laser, the filled black circles in the bottom figure of Fig. 9(a) are based on the fitting of simulated $g^{(2)}(\tau)$ because the small signal analysis fails in class-A regime. In the low-β class-B laser [Fig. 9(b)], the noise threshold $P_{\rm th}^{\rm noise}$, which is defined as Eq. (30) and represented by the yellow dashed vertical line, works very well. The noise threshold $P_{\rm th}^{\rm noise}$ perfectly agrees with the peak of the Fano factor and represents the inflection point of $g^2(0)$. On the other hand, in the low-β class-A laser [Fig. 9(a)], we do not plot the noise threshold calculated as Eq. (30) due to the failure of the small signal

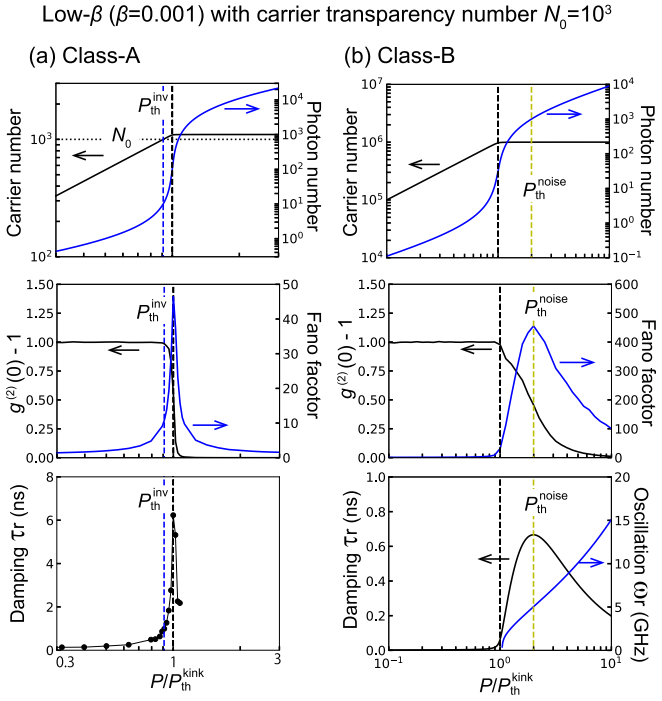

FIG. 10. Same as Fig. 9 but for low-β ($\beta = 0.001$) (a) class-A and (b) class-B lasers with a carrier transparency number $N_0 = 10^3$. The black, blue, and yellow vertical dashed lines, respectively, represent the kink P_{th}^{kink}, inversion P_{th}^{inv} and noise P_{th}^{noise} thresholds. The lifetimes are $1/\gamma_c = 1$ ns, $1/\gamma_\parallel = 0.1$ ns for (a), while $1/\gamma_c = 1$ ps, $1/\gamma_\parallel = 1$ ns for (b). These parameters lead to $\tilde{\beta} = 9.1 \times 10^{-5}$ and $\xi = 10$ for (a), while $\tilde{\beta} = 0.001$ and $\xi = 0.001$ for (b).

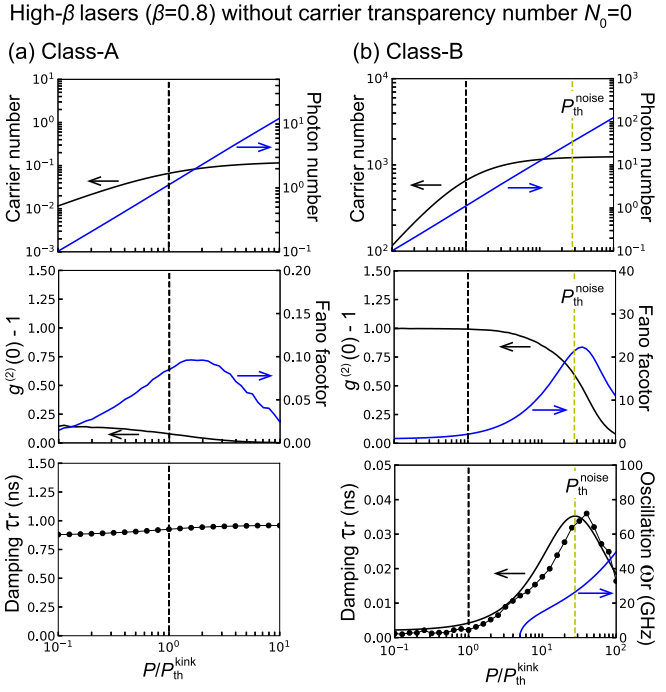

FIG. 11. Simulations for high-β ($\beta = 0.8$) (a) class-A and (b) class-B lasers without a carrier transparency number ($N_0 = 0$). Top figures: carrier number $\bar{N}$ (black line) and photon $\bar{n}$ (blue line). Middle figures: $g^{(2)}(0)$ (black line) and the Fano factor (blue line). Bottom figures: the damping time (black line or filled circles) and oscillation frequency of $g^{(2)}(\tau)$ (blue line). In the bottom figures, the black line is the result of the small signal analysis [Eq. (27)], while the black filled circles are obtained by the fitting of simulated $g^{(2)}(\tau)$. The black and yellow vertical dashed lines respectively represent the kink P_{th}^{kink} and noise P_{th}^{noise} thresholds. The lifetimes are $1/\gamma_c = 1$ ns, $1/\gamma_\parallel = 0.1$ ns for (a), while $1/\gamma_c = 1$ ps, $1/\gamma_\parallel = 1$ ns for (b).

analysis. Interestingly, even though the small signal analysis fails, the damping time of $g^2(\tau)$ behaves in the similar way as the Fano factor [compare the middle and the bottom figures in Fig. 9(a)] and the both reach their maxima at the kink threshold. Actually, in Fig. 9(a), the noise threshold is the kink threshold: $P_{th}^{noise} = P_{th}^{kink}$. The sharp change of $g^2(0)$ at the intensity kink has been experimentally confirmed in He:Ne lasers [63,64] and regarded as a textbooklike behavior [65,66].

Second, we carry out simulations with a finite carrier transparency number ($N_0 = 10^3$) and show the results for class-A [Fig. 10(a)] and class-B [Fig. 10(b)] lasers in Fig. 10. Except the carrier transparency number N_0, all the other parameters are the same as in Fig. 9. We note that the inversion thresholds are located much lower than the kink thresholds $P_{th}^{inv} \ll P_{th}^{kink}$ and they do not appear in the x-axis ranges of Fig. 10. Comparing Figs. 9 and 10, we find that N_0 does not modify photon statistics of the low-β laser a lot. For the class-B laser [see Fig. 10(b)], the negligible effect of N_0 is intuitive because the parameter $\xi = 0.001$ is very small. For the class-A laser [see Fig. 10(a)], $\xi = 10$ is not small, but N_0 does not modify the behavior of photon statistics and the sharp transition of $g^{(2)}(0)$ still exists. In the low-β class-A laser, the main effect of N_0 is the effective decrease of β. In fact, β effectively decreases by one order of magnitude as $\beta \to \tilde{\beta} \simeq 0.0001$. Thus, in Fig. 10(a), the kink of the pump-input and light-output curve is larger than that in Fig. 9(a).

In summary, in low-β lasers, the pump power dependence of $g^{(2)}(0)$ is determined mainly by the ratio $\gamma_c/\gamma_\parallel$. In class-A parameters, photon statistics sharply change from thermal to Poissonian at the kink threshold, while in class-B parameters, super-Poissonian photon statistics are present above the kink threshold.

2. High-β lasers

Now, we consider high-β lasers ($\beta = 0.8$). We show that both the ratio $\gamma_c/\gamma_\parallel$ and the carrier transparency number N_0 dramatically affect the lasing behavior of high-β lasers.

First, Fig. 11 displays the simulations of high-β class-A ($\gamma_c/\gamma_\parallel = 0.1$) [Fig. 11(a)] and class-B ($\gamma_c/\gamma_\parallel = 10^3$) [Fig. 11(b)] lasers without a carrier transparency number ($N_0 = 0$). For Fig. 11(a), the parameters are $1/\gamma_c = 1$ ns, $1/\gamma_\parallel = 0.1$ ns, $\beta = 0.8$, and $N_0 = 0$. For Fig. 11(b), the parameters are $1/\gamma_c = 1$ ps, $1/\gamma_\parallel = 1$ ns, $\beta = 0.8$, and $N_0 = 0$. Figure 11(a) indicates that the photon statistics of the high-β class-A laser without a carrier transparency number are very unconventional in that thermal photon statistics [$g^{(2)}(0) = 2$] are not recovered even far below the kink threshold. For example, even at $P = 0.1P_{th}^{kink}$, $g^{(2)}(0)$ is only around 1.2. The noise threshold also completely fails in Fig. 11(a). These photon statistics have been already mentioned in some articles in the context of high-β QD lasers with extremely high-Q

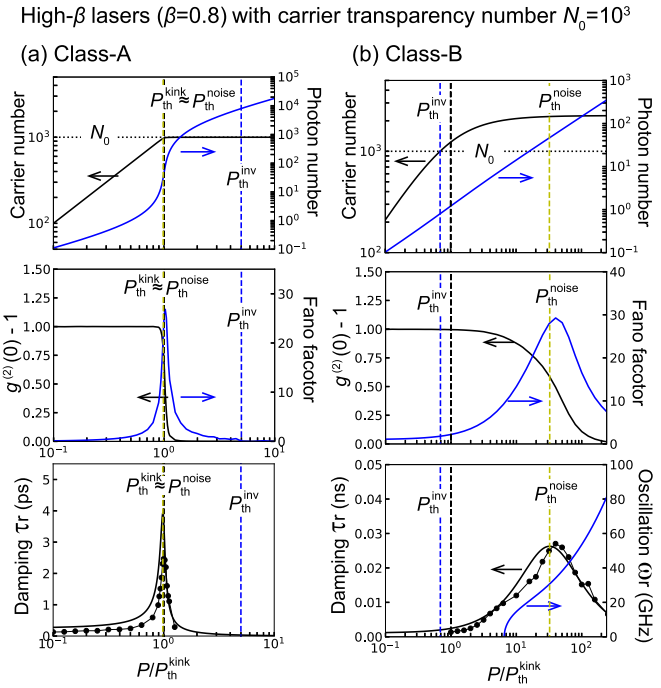

FIG. 12. Same as Fig. 11 but for high-β ($\beta = 0.8$) (a) class-A and (b) class-B lasers with a carrier transparency number $N_0 = 10^3$. The black, blue, and yellow vertical dashed lines, respectively, represent the kink P_{th}^{kink}, inversion P_{th}^{inv}, and noise P_{th}^{noise} thresholds. The lifetimes are $1/\gamma_c = 1$ ns, $1/\gamma_\parallel = 0.1$ ns for (a), while $1/\gamma_c = 1$ ps, $1/\gamma_\parallel = 1$ ns for (b). These parameters lead to $\tilde{\beta} = 5.0 \times 10^{-4}$ and $\xi = 8000$ for (a), while $\tilde{\beta} = 0.7$ and $\xi = 0.8$ for (b).

cavities [7,9,21]. The photon statistical behavior in Fig. 11(a) is attractive because the Poissonian light emission seems to be possible with an ultralow pump power. However, it will be very difficult to realize this parameter regime. The difficulty lies in that even a very small carrier transparency number breaks the photon statistical behavior shown in Fig. 11(a). For example, just with $N_0 = 50$, a class-A high-β laser will emit thermal light $g^{(2)}(0) = 2$ below the kink threshold. Therefore, the photon statistics of actual high-β and high-Q QD lasers are not like in Fig. 11(a) but will show the transition from $g^{(2)}(0) = 2$–1 [17,18]. Actually, later in Fig. 12(a), we show simulations with $N_0 = 10^3$ and a transition from $g^{(2)}(0) = 2$–1. On the other hand, the photon statistical property of the high-β class-B laser without a carrier transparency number [see Fig. 11(b)] is more familiar for us because we have already discussed the super-Poissonian tail of class-B lasers. Similarly to Fig. 7 in the main text, in the bottom figure of Fig. 11(b), the black solid line (small signal analysis) slightly deviates from the black filled circles [the fitting of $g^{(2)}(\tau)$]. This deviation originates from the imperfection of the small signal analysis. Due to this difference, the noise threshold P_{th}^{noise} underestimates the true noise threshold, but P_{th}^{noise} approximately works well. The most important consequence of Fig. 11(b) may be the fact that even though the pump-input and light-output curve is almost thresholdless, $g^{(2)}(0)$ has a threshold.

Second, we introduce a finite carrier transparency number. Figure 12 shows the simulations of high-β class-A [Fig. 12(a)] and class-B [Fig. 12(b)] lasers with $N_0 = 10^3$. All the parameters except the carrier transparency number N_0 are the same as in Fig. 11. In the class-B laser [see Fig. 12(b)], since $\xi = 0.8$ is small, the carrier transparency number $N_0 = 10^3$ does not modify the lasing properties a lot [cf. Fig. 11(b) and Fig. 12(b)]. We note that the parameter regime used in Fig. 12(b) is close to our previous experiment of the high-β buried MQW PhC laser at cryogenic temperatures [5]. Meanwhile, for the class-A laser [see Fig. 12(a)], the introduction of a finite N_0 dramatically changes both the pump-input and light-output curve and photon statistics. First, in spite of the very high $\beta(= 0.8)$, a sharp kink appears in the pump-input and light-output curve due to the small $\tilde{\beta}(= 5.0 \times 10^{-4})$ [see the top figure of Fig. 12(a)]. Additionally, the inversion threshold P_{th}^{inv} [blue dashed vertical line in Fig. 12(a)] is located clearly above the kink threshold, which is the intensity jump without inversion discussed in the main text. In terms of photon statistics, in contrast to Fig. 11(a), $g^{(2)}(0)$ sharply drops from 2 to 1 at the kink threshold in Fig. 12(a). Interestingly, $g^{(2)}(0)$ reaches a unity with a lower pump power than the inversion threshold ($P_{th}^{noise} < P_{th}^{inv}$). Therefore, the laser shown in Fig. 12(a) could be called a laser without inversion in terms not only of the intensity jump but also of photon statistics. In order to understand this phenomenon, we need to recall the fact that, in the master equation, the stimulated emission itself exists even when $G_0 < 0$. Since the stimulated emission term $\beta\gamma_\parallel \bar{N}\bar{n}$ exceeds the spontaneous emission term $\beta\gamma_\parallel \bar{N}$ at the quantum threshold, the stimulated emission can dominate over the spontaneous emission even when the G_0 is negative, which makes $g^{(2)}(0) \simeq 1$ possible below the inversion threshold. In this argument, we are assuming that the absorption process associated to $\beta\gamma_\parallel N_0 \bar{n}$ term does not affect the photon statistics.

[1] H. Yokoyama and S. D. Brorson, J. Appl. Phys. **66**, 4801 (1989).

[2] G. Bjork and Y. Yamamoto, IEEE J. Quantum Electron. **27**, 2386 (1991).

[3] M. Takiguchi, H. Sumikura, M. D. Birowosuto, E. Kuramochi, T. Sato, K. Takeda, S. Matsuo, and M. Notomi, Appl. Phys. Lett. **103**, 091113 (2013).

[4] S. Matsuo, T. Sato, K. Takeda, A. Shinya, K. Nozaki, H. Taniyama, M. Notomi, K. Hasebe, and T. Kakitsuka, IEEE J. Sel. Top. Quantum Electron. **19**, 4900311 (2013).

[5] M. Takiguchi, H. Taniyama, H. Sumikura, M. D. Birowosuto, E. Kuramochi, A. Shinya, T. Sato, K. Takeda, S. Matsuo, and M. Notomi, Opt. Exp. **24**, 3441 (2016).

[6] R. Jin, D. Boggavarapu, M. Sargent, P. Meystre, H. M. Gibbs, and G. Khitrova, Phys. Rev. A **49**, 4038 (1994).

[7] P. R. Rice and H. J. Carmichael, Phys. Rev. A **50**, 4318 (1994).
[8] N. J. van Druten, Y. Lien, C. Serrat, S. S. R. Oemrawsingh, M. P. van Exter, and J. P. Woerdman, Phys. Rev. A **62**, 053808 (2000).
[9] S. M. Ulrich, C. Gies, S. Ates, J. Wiersig, S. Reitzenstein, C. Hofmann, A. Löffler, A. Forchel, F. Jahnke, and P. Michler, Phys. Rev. Lett. **98**, 043906 (2007).
[10] C. Gies, J. Wiersig, M. Lorke, and F. Jahnke, Phys. Rev. A **75**, 013803 (2007).
[11] J. Wiersig, C. Gies, F. Jahnke, M. Aßmann, T. Berstermann, M. Bayer, C. Kistner, S. Reitzenstein, C. Schneider, S. Höfling *et al.*, Nature (London) **460**, 245 (2009).
[12] D. Elvira, X. Hachair, V. B. Verma, R. Braive, G. Beaudoin, I. Robert-Philip, I. Sagnes, B. Baek, S. W. Nam, E. A. Dauler, I. Abram, M. J. Stevens, and A. Beveratos, Phys. Rev. A **84**, 061802(R) (2011).
[13] M. Khajavikhan, A. Simic, M. Katz, J. Lee, B. Slutsky, A. Mizrahi, V. Lomakin, and Y. Fainman, Nature (London) **482**, 204 (2012).
[14] Y. Ota, K. Watanabe, S. Iwamoto, and Y. Arakawa, Phys. Rev. A **89**, 023824 (2014).
[15] P. Hamel, S. Haddadi, F. Raineri, P. Monnier, G. Beaudoin, I. Sagnes, A. Levenson, and A. M. Yacomotti, Nature Photon. **9**, 311 (2015).
[16] C. Redlich, B. Lingnau, S. Holzinger, E. Schlottmann, S. Kreinberg, C. Schneider, M. Kamp, S. Höfling, J. Wolters, S. Reitzenstein, and K. Lüdge, New J. Phys. **18**, 063011 (2016).
[17] Y. Ota, M. Kakuda, K. Watanabe, S. Iwamoto, and Y. Arakawa, Opt. Exp. **25**, 19981 (2017).
[18] S. Kreinberg, W. W. Chow, J. Wolters, C. Schneider, C. Gies, F. Jahnke, S. Höfling, M. Kamp, and S. Reitzenstein, Light: Sci. & Amp; Appl. **6**, e17030 (2017).
[19] S. T. Jagsch, N. V. Triviño, F. Lohof, G. Callsen, S. Kalinowski, I. M. Rousseau, R. Barzel, J.-F. Carlin, F. Jahnke, R. Butté *et al.*, Nature Commun. **9**, 564 (2018).
[20] J. Mork and G. L. Lippi, Appl. Phys. Lett. **112**, 141103 (2018).
[21] B. Gulyak, B. Melcher, and J. Wiersig, Phys. Rev. A **98**, 053857 (2018).
[22] I. Prieto, J. M. Llorens, L. E. M. noz Camúñez, A. G. Taboada, J. Canet-Ferrer, J. M. Ripalda, C. Robles, G. M. noz Matutano, J. P. Martínez-Pastor, and P. A. Postigo, Optica **2**, 66 (2015).
[23] G. Björk, A. Karlsson, and Y. Yamamoto, Phys. Rev. A **50**, 1675 (1994).
[24] Y. Yamamoto and G. Björk, Japanese J. Appl. Phys. **30**, L2039 (1991).
[25] N. Takemura, J. Omachi, and M. Kuwata-Gonokami, Phys. Rev. A **85**, 053811 (2012).
[26] A. Lebreton, I. Abram, N. Takemura, M. Kuwata-Gonokami, I. Robert-Philip, and A. Beveratos, New J. Phys. **15**, 033039 (2013).
[27] Y. Lien, S. M. de Vries, N. J. van Druten, M. P. van Exter, and J. P. Woerdman, Phys. Rev. Lett. **86**, 2786 (2001).
[28] H. F. Hofmann and O. Hess, Phys. Rev. A **62**, 063807 (2000).
[29] H. F. Hofmann and O. Hess, J. Opt. Soc. Am. B **17**, 1926 (2000).
[30] T. Ogawa, Phys. Rev. A **42**, 4210 (1990).
[31] P. Paoli, A. Politi, and F. T. Arecchi, Z. Phys. B Condens. Matter **71**, 403 (1988).
[32] A. Moelbjerg, P. Kaer, M. Lorke, B. Tromborg, and J. Mørk, IEEE J. Quantum Electron. **49**, 945 (2013).
[33] F. Arecchi, G. Lippi, G. Puccioni, and J. Tredicce, Opt. Commun. **51**, 308 (1984).
[34] F. T. Arecchi and R. G. Harrison, *Instabilities and Chaos in Quantum Optics* (Springer Science & Business Media, New York, 2012), Vol. 34.
[35] T. Wang, G. Puccioni, and G. Lippi, Sci. Rep. **5**, 15858 (2015).
[36] A. Auffèves, J.-M. Gérard, and J.-P. Poizat, Phys. Rev. A **79**, 053838 (2009).
[37] H. Sumikura, E. Kuramochi, H. Taniyama, and M. Notomi, Phys. Rev. B **94**, 195314 (2016).
[38] D. E. McCumber, Phys. Rev. **141**, 306 (1966).
[39] K. Roy-Choudhury, S. Haas, and A. F. J. Levi, Phys. Rev. Lett. **102**, 053902 (2009).
[40] G. P. Puccioni and G. L. Lippi, Opt. Express **23**, 2369 (2015).
[41] D. T. Gillespie, J. Comput. Phys. **22**, 403 (1976).
[42] D. T. Gillespie, J. Phys. Chem. **81**, 2340 (1977).
[43] A. Verger, C. Ciuti, and I. Carusotto, Phys. Rev. B **73**, 193306 (2006).
[44] M. O. Scully and W. E. Lamb, Phys. Rev. **166**, 246 (1968).
[45] T. Fink, A. Schade, S. Höfling, C. Schneider, and A. Imamoglu, Nature Phys. **14**, 365 (2017).
[46] R. Loudon, *The Quantum Theory of Light*, 3rd ed. (Oxford University Press, Oxford, 2000).
[47] S. E. Harris, Phys. Rev. Lett. **62**, 1033 (1989).
[48] M. O. Scully and M. S. Zubairy, *Quantum Optics* (Cambridge University Press, Cambridge, 1999).
[49] A. Imamoglu, R. J. Ram, S. Pau, and Y. Yamamoto, Phys. Rev. A **53**, 4250 (1996).
[50] G. Malpuech, A. Kavokin, A. Di Carlo, and J. J. Baumberg, Phys. Rev. B **65**, 153310 (2002).
[51] H. Deng, G. Weihs, D. Snoke, J. Bloch, and Y. Yamamoto, Proc. Nat. Acad. Sci. **100**, 15318 (2003).
[52] W. W. Chow, F. Jahnke, and C. Gies, Light: Science & Amp; Appl. **3**, e201 (2014).
[53] T. P. Pearsall, *GaInAsP Alloy Semiconductors* (John Wiley & Sons, New York, 1982).
[54] B. Sermage, J. P. Heritage, and N. K. Dutta, J. Appl. Phys. **57**, 5443 (1985).
[55] Y. Ishitani, J. Appl. Phys. **86**, 6816 (1999).
[56] A. Yariv, Appl. Phys. Lett. **53**, 1033 (1988).
[57] Low-β class-A lasers can be approximated by the van der Pol-like equation of the electric field. Using the Fokker-Planck equation, we can obtain the steady-state distribution and prove $g^{(2)}(0) = \pi/2$ at the lasing threshold. For example, see chap, 9 in Ref. [67].
[58] V. DeGiorgio and M. O. Scully, Phys. Rev. A **2**, 1170 (1970).
[59] R. Graham and H. Haken, Z. Phys. **237**, 31 (1970).
[60] F. Lohof, R. Barzel, P. Gartner, and C. Gies, Phys. Rev. Appl. **10**, 054055 (2018).
[61] L. D. Landau, E. M. Lifshitz, and L. Pitaevskii, *Statistical Physics*, Part I (Elsevier, Amsterdam, 1980).
[62] M. O. Scully and W. E. Lamb, Phys. Rev. **159**, 208 (1967).
[63] F. Arecchi, G. Rodari, and A. Sona, Phys. Lett. A **25**, 59 (1967).
[64] F. Davidson and L. Mandel, Phys. Lett. A **25**, 700 (1967).
[65] L. Mandel and E. Wolf, *Optical Coherence and Quantum Optics* (Cambridge University Press, Cambridge, 1995).
[66] H. Haken, *Laser Theory* (Springer Science & Business Media, New York, 2012).
[67] C. Gardiner and P. Zoller, *Quantum Noise* (Springer Science & Business Media, New York, 2004), Vol. 56.